

Handbook of Numerical Analysis

Volume 23

# Numerical Control: Part A

---

Edited by

**Emmanuel Trélat**

Sorbonne Université

Laboratoire Jacques-Louis Lions

Paris, France

**Enrique Zuazua**

Department of Data Science

Friedrich-Alexander-Universität Erlangen-Nürnberg (FAU)

Erlangen, Germany

Fundación Deusto

Bilbao, Basque Country, Spain

Universidad Autónoma de Madrid

Madrid, Spain



**North-Holland**

An imprint of Elsevier

## Chapter 15

# Data-driven modeling and control of large-scale dynamical systems in the Loewner framework

## Methodology and applications

Ion Victor Gosea<sup>a,\*</sup>, Charles Poussot-Vassal<sup>b</sup>, and Athanasios C. Antoulas<sup>c,d,e</sup>

<sup>a</sup>*Data-Driven System Reduction and Identification (DRI) Group, Max Planck Institute (MPI), Magdeburg, Germany,* <sup>b</sup>*Information Processing and Systems Department, ONERA, Toulouse, France,* <sup>c</sup>*Electrical and Computer Engineering (ECE) Department, Rice University, Houston, TX, United States,* <sup>d</sup>*Max Planck Institute, Magdeburg, Germany,* <sup>e</sup>*Baylor College of Medicine, Houston, TX, United States*

\*Corresponding author: e-mail address: [gosea@mpi-magdeburg.mpg.de](mailto:gosea@mpi-magdeburg.mpg.de)

## Contents

<b>1 Introduction: data-driven modeling and control</b>	<b>500</b>	3.2 Ground vibration tests on business jet aircraft	520
<b>2 The Loewner framework for data-driven modeling: an overview</b>	<b>502</b>	3.3 Hydroelectricity open-channel benchmark	521
2.1 Generalities on the Loewner framework and model structures	502	<b>4 Control in the Loewner framework</b>	<b>523</b>
2.2 The Loewner framework in the LTI case	504	4.1 Data-driven control, virtual reference model and <b>L-DDC</b> rationale	523
2.3 Generalizations to parametric linear systems	507	4.2 Pulsed fluidic actuator control	524
2.4 Generalization to modeling from time-domain data	510	4.3 Transport phenomena benchmark	525
2.5 Extensions to nonlinear systems	514	4.3.1 A model-driven approximation and control	526
<b>3 Model reduction examples (large-scale systems)</b>	<b>518</b>	4.3.2 Data-driven control	526
3.1 Gust load oriented generic business jet aircraft model	518	<b>5 Summary and conclusions</b>	<b>527</b>
		References	528

---

**Abstract**

In this contribution we discuss the modeling and model reduction framework known as the Loewner framework. This is a data-driven approach, applicable to large-scale systems, which was originally developed for applications to linear time-invariant systems. In recent years, this method has been extended to a number of additional more complex scenarios, including linear parametric or nonlinear dynamical systems. We will provide here an overview of the latter two, together with time-domain extensions. Additionally, the application of the Loewner framework is illustrated by a collection of practical test cases. Firstly, for data-driven complexity reduction of the underlying model, and secondly, for dealing with control applications of complex systems (in particular, with feedback controller design).

**Keywords**

Data-driven modeling, Data-driven control, Loewner matrix, Rational approximation, Interpolation-based methods, Complex systems, Feedback controller design, Linear systems, Parametrized systems, Bilinear systems, Time-domain data, Time-delay systems

**MSC Codes**

93A15, 93A30, 93B11, 93B15, 93B52, 93C05, 93C10, 93C15

---

## 1 Introduction: data-driven modeling and control

The physical complexity of dynamical systems describing time-dependent processes stems from underlying non-linearities, the coupling dynamics, or the large amount of degrees of freedom (variables or parameters). The latter aspect is also related to enforcing specific accuracy requirements, that yield models of large dimension which are hence challenging to use for control purposes or for numerical simulations.

Simulating such complex dynamical systems is currently a common feature of many numerical software toolboxes, and is widely used both in industry and in academia. As numerical simulations become more involved, processing of increased amounts of data is required. Consequently, the number of variables under analysis is limited to the physical ones (even in the era of machine learning), while the rest are discarded. Computing simplified, easy to use dynamical models is one purpose of the model approximation and reduction discipline. Such models may then be used in a many query optimization and simulation process. That is why it is of critical importance to construct reliable surrogate models. Model reduction typically refers to a class of methodologies used for reducing the computational complexity of large-scale models of dynamical systems. The goal generally is to approximate the original system with a smaller and simpler system with the same structure and similar response characteristics as the original. For an overview of model reduction methods, we refer the reader to Antoulas (2005); Benner et al. (2015, 2017); Antoulas et al. (2020a), and to the references therein. In many practical scenarios, a complete mathematical

description of the dynamical system under study is not always available or not fully known. Instead of depending only on physical laws (describing partial or ordinary differential equations), one can infer important properties of the system directly from measured or computed data.

With the increasing emergence of data-driven applications in many fields of the applied sciences, the need for incorporating measurements in the modeling and controlling stage has steadily grown over the last decades. The main challenge consists in using the available data in order to effectively construct surrogate models or controllers. In this latter case, the controller has to be designed based on experimental measurements, instead of a model description. Model-based methods can hence be replaced by data-driven strategies that construct the controller, directly from experimental data. Such techniques are also known as direct methods and can be useful when control-oriented models are either too complex or too costly to obtain.

The Loewner Framework (LF) is a data-driven model identification and reduction technique that was originally introduced in Mayo and Antoulas (2007). It is based on the Loewner-matrix interpolation method elaborated by the third author of the current paper, more than 20 years earlier, in the seminal contribution (Antoulas and Anderson, 1986). Using only measured data, the LF constructs surrogate models directly and with low computational effort. For recent tutorial papers on LF applied to linear dynamical systems, we refer the reader to Antoulas et al. (2017); Karachalios et al. (2020a). Extensions that use time-domain data were provided in Ionita and Antoulas (2012); Antoulas et al. (2018) (for a Hankel matrix approach) as well as in Peherstorfer et al. (2017) (for inferring transfer function measurements from time series). The Loewner framework has been recently extended to certain classes of nonlinear systems, such as bilinear systems in Antoulas et al. (2016a), and quadratic-bilinear systems in Gosea and Antoulas (2015, 2018). An adaptive extension of the original Loewner-based method in Antoulas and Anderson (1986), named the AAA (Adaptive-Antoulas-Anderson) algorithm, was recently proposed in Nakatsukasa et al. (2018); it is a data-driven rational approximation method that combines interpolation and least-squares (LS) fitting.

In the first part of this contribution, the Loewner framework is mainly used as a model identification and reduction tool. In the second part, the same framework is used for feedback controller design. In the proposed setup, the reference controller is not computed by means of a given model, but using input-output data of the system. Consequently, the Loewner framework is used for synthesizing a controller directly from measured data, which shows that it is also a data-driven control tool. Data-driven control strategies consist in recasting the control design problem as an identification one. By doing so, the model simplification process is shifted directly to the controller design step. The Loewner-based data-driven control methodology was extensively studied in recent years, starting with the original contribution (Kergus et al., 2017) and subsequently with Vuillemin et al. (2020); Gosea et al. (2021b); Poussot-Vassal et al. (2021a,b).

The main philosophy of the Loewner framework is as follows: starting with frequency response measurements (or, alternatively, with time-domain sequences of measured inputs and outputs), the data are arranged in a specific matrix format. Then, the dominant characteristics of the model are extracted by means of an appropriate projection (by means of SVD's). Thus, simplified / reduced surrogate models can be computed without access to system's description. Such models typically need to preserve some of the original system's properties, such as stability or passivity. In what follows we will also cover practical issues such as stability preservation/enforcement, as presented in Gosea and Antoulas (2016).

We denote by  $\mathbb{R}$  (resp.  $\mathbb{C}$ ) the set of real (resp. complex) numbers,  $\mathbb{C}_+$  ( $\mathbb{C}_-$ ) the open right (left) half plane and the complex variable by  $\iota = \sqrt{-1}$ . Let  $\Lambda_{(\mathbf{A}, \mathbf{E})} = \{z \in \mathbb{C} \mid \det(z\mathbf{E} - \mathbf{A}) = 0\}$  denote the set of singularities of the pencil  $(\mathbf{A}, \mathbf{E})$  and, more generally, let  $\Lambda_{\mathbf{H}}$  denote the set of isolated singularities of the complex function  $\mathbf{H}$ .

The paper is organized as follows: after the introduction on data-driven modeling and control in Section 1, we continue with an overview on the Loewner framework for data-driven modeling in Section 2 with various subsections that cover specific extensions of the framework. Section 3 contains three model reduction examples in the Loewner framework, while Section 4 deals with the Loewner data-driven control rationale. This illustrates how the Loewner tool can be effective for both model-based or data-driven control approaches. Finally, 5 contains the concluding remarks together with a short summary of the paper.

## 2 The Loewner framework for data-driven modeling: an overview

### 2.1 Generalities on the Loewner framework and model structures

The Loewner framework is a data-driven method aimed at building a time invariant differential algebraic equation model / realization, with associated transfer function  $\mathbf{H}_{\mathcal{I}}$  or  $\mathbf{H}^{(\mathcal{I})}$  (defined later). This model interpolates data obtained from experimental measurements or the evaluation of a (collection of) transfer function(s). As made clearer later in this section, according to the mathematical structure and nature of the underlying system,  $\mathbf{H}_{\mathcal{I}}$  has some specific properties.

Although in this section we mainly focus on the Loewner framework as a system identification tool, *i.e.*, by achieving (rational) interpolation properties, the main application of the method is indeed for model reduction purposes (when frequency response data are available). This will be illustrated in the third part of the manuscript, *i.e.*, in Section 3, with several examples of applying model order reduction. The model approximation and reduction provided in the Loewner framework is granted by means of numerical compression of the interpolation data (using a singular value decomposition). In this way, the compressed model attains similar interpolation properties as the uncompressed raw data model, but at the same time, it is of reduced order. Choosing a truncation

value is often dictated by the application, and it is typically done as a compromise between enforcing high approximation quality at the cost of increasing the dimension of the compressed data models.

In its original form presented in Mayo and Antoulas (2007),  $\mathbf{H}^{(N)} (\mathcal{J} = \{N\})$  is a descriptor linear time invariant (**LTI**) dynamical model with transfer function  $\mathbf{H}^{(N)} : \mathbb{C} \setminus \Lambda_{(\mathbf{A}, \mathbf{E})} \rightarrow \mathbb{C}^{p \times m}$ , where  $N \in \mathbb{N}$  denotes the number of collected data. We also denote with  $\mathbf{H}_n$  the transfer function with McMillan degree  $n$  ( $\mathcal{I} = \{n\}$ ). A complete description of this case is available in the recent surveys (Antoulas et al., 2017; Karachalios et al., 2020a). Extension to parametric **LTI** (**pLTI**) model structure also exists (Ionita and Antoulas, 2014). In this case, one obtains a multi-valued rational and polynomial transfer function  $\mathbf{H}^{(N, M)} : (\mathbb{C} \times \mathbb{R}) \setminus \Lambda_{\mathbf{H}^{(N, M)}} \rightarrow \mathbb{C}^{p \times m}$  where  $\mathcal{J} = \{N, M\}$  data are used (or  $\mathbf{H}_{r, q}$ , where  $\mathcal{I} = \{r, q\}$ ), where  $M \in \mathbb{N}$  is the number of data along the parameter variable (and  $q \in \mathbb{N}$  is the rational and polynomial order along the parameter). The resulting function both interpolates the complex and real parametric variables. From a different perspective, extensions to nonlinear model structures have also been investigated. Among them, one can mention the bilinear and/or quadratic forms, explored in a series of papers (Gosea and Antoulas, 2015; Antoulas et al., 2016a; Gosea and Antoulas, 2018; Antoulas et al., 2019; Gosea et al., 2021a; Antoulas et al., 2020b). In these cases, the associated transfer function is a collection of multivariate coupled infinite cascade of linear systems reading as  $\mathbf{H}^{(N_1)} : \mathbb{C} \setminus \Lambda_{\mathbf{H}^{(N_1)}} \rightarrow \mathbb{C}^{p \times m}$ ,  $\mathbf{H}^{(N_1, N_2)} : (\mathbb{C} \times \mathbb{C}) \setminus \Lambda_{\mathbf{H}^{(N_1, N_2)}} \rightarrow \mathbb{C}^{p \times m}$  and  $\mathbf{H}^{(N_1, N_2, \dots)} : (\mathbb{C} \times \mathbb{C} \times \dots) \setminus \Lambda_{\mathbf{H}^{(N_1, N_2, \dots)}} \rightarrow \mathbb{C}^{p \times m}$  ( $\mathcal{J} = \{N_1, N_2, \dots\}$ ). The Loewner interpolation framework seeks a function interpolating the  $N_1, N_2, \dots$  data along each related multi-valued transfer functions  $\mathbf{H}^{(N_1)}, \mathbf{H}^{(N_1, N_2, \dots)}$  ( $N_1, N_2, \dots \in \mathbb{N}$ ). Similarly, we denote with  $\mathbf{H}_{r_1, r_2, \dots}$  the associated transfer function of order  $r_1, r_2, \dots \in \mathbb{N}$ .

In all the cases mentioned here, the transfer function (or the set of transfer functions) is rational and polynomial, and it interpolates the data. In comparison to realization-driven model reduction, data-driven methods based on interpolation construct models that match the original transfer function(s) at well chosen points in the complex plane (also denoted as support points for barycentric representations (Berrut and Trefethen, 2006; Nakatsukasa et al., 2018)). As such, it provides a generalization of the Padé method to an arbitrary (set of) point(s). Data-driven methods based on rational and polynomial interpolation benefit also from the fact that it only requires the transfer function evaluation, whereas projection methods require the internal model (system matrices or operators). The latter are thus referred to as *intrusive* methods, while the former are *non-intrusive* or *data-driven* ones. In this section, a review of the Loewner framework is provided, together with some of its extensions. More specifically, Section 2.2 presents the Loewner framework in its original form, leading to a linear time invariant model. Extensions to linear parametric and to bilinear systems are sequentially illustrated in Sections 2.3 and 2.5. As a direct extension,

the time-domain Loewner, dealing with sampled time-domain data instead of frequency domain data, is covered in Section 2.4.

## 2.2 The Loewner framework in the LTI case

The main ingredient of the Loewner framework is summarized next in the multi-input multi-output (**MIMO**) **LTI** case (Antoulas, 2005, chap. 4). Let us consider this system to be a  $m$  inputs  $p$  outputs dynamical one described by a  $n$ -th order differential algebraic equation (**DAE**) model  $\mathcal{S} : (\mathbf{E}, \mathbf{A}, \mathbf{B}, \mathbf{C}, \mathbf{0})^1$  which explicitly reads as  $\dot{\mathbf{x}}(t) = \mathbf{Ax}(t) + \mathbf{Bu}(t)$ ,  $\mathbf{y}(t) = \mathbf{Cx}(t)$ , where  $\mathbf{E}, \mathbf{A} \in \mathbb{R}^{n \times n}$ ,  $\mathbf{B} \in \mathbb{R}^{n \times m}$ ,  $\mathbf{C} \in \mathbb{R}^{p \times n}$ . Its associated transfer function  $\mathbf{H} : \mathbb{C} \setminus \Lambda_{(\mathbf{A}, \mathbf{E})} \rightarrow \mathbb{C}^{p \times m}$  is

$$\mathbf{H}(\xi) = \mathbf{C}\Phi(\xi)\mathbf{B} \text{ where } \Phi(\xi) = (\xi\mathbf{E} - \mathbf{A})^{-1} \in \mathbb{C}^{n \times n}. \quad (1)$$

Importantly, as any rational and polynomial function, relation (1) can be characterized in its Lagrangian basis with distinct Lagrange nodes (or support points)  $\lambda_i \in \mathbb{C} \setminus \Lambda_{(\mathbf{A}, \mathbf{E})}$ . Then one can rewrite it in its barycentric formula form as follows (for  $\alpha_i \neq 0$ ),  $\mathbf{H}(\xi) = \sum_{i=1}^{n+1} \beta_i \mathbf{q}_i(\xi) / \sum_{i=1}^{n+1} \alpha_i \mathbf{q}_i(\xi)$  where  $\mathbf{q}_i(\xi) = 1/(\xi - \lambda_i)$ . Let this system generate right (column) data together with left (row) data, as

$$(\lambda_i, \mathbf{r}_i, \mathbf{w}_i) \text{ for } i = 1, \dots, \bar{n} \text{ and } (\mu_j, \mathbf{l}_j^T, \mathbf{v}_j^T) \text{ for } j = 1, \dots, \underline{n}, \quad (2)$$

where  $\mathbf{w}_i = \mathbf{H}(\lambda_i)\mathbf{r}_i$  and  $\mathbf{v}_j^T = \mathbf{l}_j^T \mathbf{H}(\mu_j)$ , with  $\mathbf{r}_i \in \mathbb{C}^{m \times 1}$ ,  $\mathbf{l}_j \in \mathbb{C}^{p \times 1}$ ,  $\mathbf{w}_i \in \mathbb{C}^{p \times 1}$ , and  $\mathbf{v}_j \in \mathbb{C}^{m \times 1}$  ( $m, p \geq 1$ ). In addition, we define the set of distinct interpolation points  $\{z_k\}_{k=1}^N \subset \mathbb{C}$ , leading to responses  $\{\Phi_k\}_{k=1}^N \in \mathbb{C}^{p \times m}$ , rearranged as follows ( $N = \bar{n} + \underline{n}$ ),

$$\{z_k\}_{k=1}^N = \{\lambda_i\}_{i=1}^{\bar{n}} \cup \{\mu_j\}_{j=1}^{\underline{n}} \text{ and } \{\Phi_k\}_{k=1}^N = \{\Phi_i\}_{i=1}^{\bar{n}} \cup \{\Phi_j\}_{j=1}^{\underline{n}}. \quad (3)$$

The method then consists in building the *Loewner* matrix  $\mathbb{L} \in \mathbb{C}^{n \times \bar{n}}$  and *shifted Loewner* matrix  $\mathbb{M} \in \mathbb{C}^{\bar{n} \times \underline{n}}$  defined as follows, for  $i = 1, \dots, \bar{n}$  and  $j = 1, \dots, \underline{n}$ :

$$\begin{aligned} \mathbb{L}_{(j,i)} &= \frac{\mathbf{v}_j^T \mathbf{r}_i - \mathbf{l}_j^T \mathbf{w}_i}{\mu_j - \lambda_i} = \frac{\mathbf{l}_j^T (\mathbf{H}(\mu_j) - \mathbf{H}(\lambda_i)) \mathbf{r}_i}{\mu_j - \lambda_i}, \\ \mathbb{M}_{(j,i)} &= \frac{\mu_j \mathbf{v}_j^T \mathbf{r}_i - \lambda_i \mathbf{l}_j^T \mathbf{w}_i}{\mu_j - \lambda_i} = \frac{\mathbf{l}_j^T (\mu_j \mathbf{H}(\mu_j) - \lambda_i \mathbf{H}(\lambda_i)) \mathbf{r}_i}{\mu_j - \lambda_i}. \end{aligned} \quad (4)$$

Additionally, let  $\mathbb{W} = [\mathbf{w}_1, \dots, \mathbf{w}_{\bar{n}}]$  and  $\mathbb{V} = [\mathbf{v}_1, \dots, \mathbf{v}_{\underline{n}}]^T$ . Finally, let  $\mathbf{\Lambda} = \text{diag}(\lambda_1, \dots, \lambda_{\bar{n}})$ ,  $\mathbf{M} = \text{diag}(\mu_1, \dots, \mu_{\underline{n}})$ ,  $\mathbf{R} = [\mathbf{r}_1, \dots, \mathbf{r}_{\bar{n}}]$ , and  $\mathbf{L} =$

<sup>1</sup> Fixing the last component to zero is not restrictive: see e.g. Karachalios et al. (2020a) where the direct feed-through term is equivalently incorporated in the  $\mathbf{E}$  matrix.

$[I_1, \dots, I_n]$ . The following Sylvester equations (Antoulas, 2005, chap. 6) are hence satisfied by the Loewner  $\mathbb{L}$  and shifted Loewner  $\mathbb{M}$  matrices:

$$\mathbb{M}\mathbb{L} - \mathbb{L}\mathbb{A} = \mathbb{V}\mathbb{R} - \mathbb{L}\mathbb{W} \text{ and } \mathbb{M}\mathbb{M} - \mathbb{M}\mathbb{A} = \mathbb{M}\mathbb{V}\mathbb{R} - \mathbb{L}\mathbb{W}\mathbb{A}. \quad (5)$$

Then, the descriptor realization  $\mathcal{S}^{(N)}$  is given as,<sup>2</sup>

$$\mathbf{E}^{(N)}\dot{\mathbf{x}}(t) = \mathbf{A}^{(N)}\mathbf{x}(t) + \mathbf{B}^{(N)}\mathbf{u}(t), \mathbf{y}(t) = \mathbf{C}^{(N)}\mathbf{x}(t), \quad (6)$$

where  $\mathbf{E}^{(N)} = -\mathbb{L} \in \mathbb{C}^{\underline{n} \times \bar{n}}$ ,  $\mathbf{A}^{(N)} = -\mathbb{M} \in \mathbb{C}^{\underline{n} \times \bar{n}}$ ,  $\mathbf{B}^{(N)} = \mathbb{V} \in \mathbb{C}^{\underline{n} \times m}$ , and  $\mathbf{C}^{(N)} = \mathbb{W} \in \mathbb{C}^{p \times \bar{n}}$  and which associated transfer function  $\mathbf{H}^{(N)} : \mathbb{C} \setminus \Lambda_{(\mathbb{L}, \mathbb{M})} \rightarrow \mathbb{C}^{p \times m}$  ( $A^+$  denotes the Moore–Penrose pseudo-inverse of  $A$ )

$$\mathbf{H}^{(N)}(\xi) = \mathbf{C}^{(N)}\Phi^{(N)}(\xi)\mathbf{B}^{(N)} \text{ where } \Phi^{(N)}(\xi) = (\xi\mathbf{E}^{(N)} - \mathbf{A}^{(N)})^+ \in \mathbb{C}^{\bar{n} \times \bar{n}} \quad (7)$$

tangentially interpolates  $\mathbf{H}$  at the given support points and directions defined in (2), *i.e.* satisfies the conditions

$$\mathbf{H}^{(N)}(\lambda_i)\mathbf{r}_i = \mathbf{H}(\lambda_i)\mathbf{r}_i \text{ and } \mathbf{l}_j^T \mathbf{H}^{(N)}(\mu_j) = \mathbf{l}_j^T \mathbf{H}(\mu_j). \quad (8)$$

Note that  $\mathbf{H}^{(N)}$  is an interpolant of the data without any reduction. It refers to the realization constructed using the  $N$  available data.

From now on, let us assume that  $\underline{n} = \bar{n}$ , also referred to as the square case.<sup>3</sup> Moreover, assuming that the number  $N = \underline{n} + \bar{n}$  of available data is large enough, then it was shown in Mayo and Antoulas (2007) that a minimal model  $\mathbf{H}_r$  of dimension  $r < \bar{n} = \underline{n}$  still satisfying the interpolatory conditions (8) can be computed by projecting the realization (6), provided that the following holds (for  $k = 1, \dots, N$ )<sup>4</sup>

$$\text{rank}(z_k \mathbb{L} - \mathbb{M}) = \text{rank}([\mathbb{L}, \mathbb{M}]) = \text{rank}([\mathbb{L}^H, \mathbb{M}^H]^H) = r, \quad (9)$$

where  $z_k$  are as in (3). Let  $\mathbf{Y} \in \mathbb{C}^{\underline{n} \times r}$  (resp.  $\mathbf{X} \in \mathbb{C}^{\bar{n} \times r}$ ) be the matrix containing the first  $r$  left (resp. right) singular vectors of  $[\mathbb{L}, \mathbb{M}]$  (resp.  $[\mathbb{L}^H, \mathbb{M}^H]^H$ ). Then,  $\mathcal{S}_r : (\mathbf{E}_r, \mathbf{A}_r, \mathbf{B}_r, \mathbf{C}_r, \mathbf{0})$  where

$$\mathbf{E}_r = \mathbf{Y}^H \mathbf{E}^{(N)} \mathbf{X}, \mathbf{A}_r = \mathbf{Y}^H \mathbf{A}^{(N)} \mathbf{X}, \mathbf{B}_r = \mathbf{Y}^H \mathbf{B}^{(N)} \text{ and } \mathbf{C}_r = \mathbf{C}^{(N)} \mathbf{X}, \quad (10)$$

is a descriptor realization of  $\mathbf{H}_r$ , given as  $\mathbf{H}_r(\xi) = \mathbf{C}_r \Phi_r(\xi) \mathbf{B}_r$  where  $\Phi_r(\xi) = (\xi \mathbf{E}_r - \mathbf{A}_r)^{-1} \in \mathbb{C}^{r \times r}$  encoding a *minimal McMillan degree* equal to  $v = \text{rank}(\mathbb{L})$ . Note that if  $r$  in (9) is greater than  $\text{rank}(\mathbb{L})$ , then  $\mathbf{H}_r$  may either have

<sup>2</sup> The upper case letter  $N$  as superscript denotes here the number of considered data used to construct the realization.

<sup>3</sup> The term square refers to the square shape of the dynamic matrices  $\mathbf{A}$  and  $\mathbf{E}$ .

<sup>4</sup> The lower case letter  $r$  as subscript denotes here the dimension of the realization instead of the number of data measurements (denoted with the upper case letter  $N$ ).

a direct feed-through term or a polynomial part. Finally, the number  $r$  of singular vectors composing  $\mathbf{Y}$  and  $\mathbf{X}$  used to project the system  $\mathbf{H}_r$  in (10) may be decreased at the cost of imposing an approximate interpolation of data, leading to the reduced order rational and polynomial model. This allows a trade-off between complexity of the resulting model and accuracy of the interpolation. The Loewner framework thus is a landmark appropriate for identification, approximationm and order reduction. Let us close this first part with two linear differential algebraic equations examples where the Loewner framework is applied. Both continuous and sampled-time cases are considered, highlighting how versatile this landmark is. More detailed, didactic examples are found in surveys (Antoulas et al., 2017; Karachalios et al., 2020a).

**Remark 1.** Because of its data-driven nature, the Loewner framework produces reduced-order models for which the approximation quality strongly depends on the data used in the process. One of the main attributes of the method is that it compresses the available information (interpolation conditions) and extracts relevant information. Moreover, it has been recently shown in Antoulas et al. (2017), Section 2.1.10, that the projected model indeed satisfies particular interpolation properties. There, the left and right interpolation points, values, and directions are explicitly provided for the projected Loewner model.

**Remark 2.** Other data-driven approaches such as the AAA algorithm (Nakatsukasa et al., 2018) enforce interpolation at particular data points, based on a greedy selection scheme. In this way, an indication of where to interpolate is provided.

**Example 1** (Continuous-time rational and polynomial model interpolation). We consider the rational and polynomial model  $\mathbf{H}(s) = s + 1/(s + 1) = (s^2 + s + 1)/(s + 1)$  with a realization  $\mathcal{S} : (\mathbf{E}, \mathbf{A}, \mathbf{B}, \mathbf{C}, \mathbf{0})$  given by:  $\mathbf{E} = [0\ 1\ 0; 0\ 0\ 1; 0\ 0\ 1]$ ,  $\mathbf{A} = [1\ 0\ 0; 0\ 1\ 0; 0\ 0 - 1]$ ,  $\mathbf{B}^T = [0\ 0\ 1]$ , and  $\mathbf{C} = [1\ 1\ 1]$ . By sampling  $\mathbf{H}$  along  $\lambda_i = \{1, 3, 5, 7\}$  and  $\mu_j = \{2, 4, 6, 8\}$  with tangential directions  $\mathbf{r}_i = \mathbf{l}_j = 1$  for  $i, j = 1, \dots, 4 = \bar{n} = \underline{n}$  ( $N = 8$ ) leads to the measurements  $\mathbf{w}_i = \{3/2, 13/4, 31/6, 57/8\}$  and  $\mathbf{v}_j = \{7/3, 21/5, 43/7, 73/9\}$ . Constructing the Loewner matrices as in (4), one obtains a 4-th order realization  $\mathcal{S}_N : (-\mathbb{L}, -\mathbb{M}, \mathbb{V}, \mathbb{W})$ . Following (9), the rank of the  $[\mathbb{L}, \mathbb{M}]$  matrix is equal to  $r = 3$ . Computing the **SVD** of the  $[\mathbb{L}, \mathbb{M}]$  matrix leads to the following normalized singular values  $\sigma = \{1, 5.59 \cdot 10^{-2}, 6.8804 \cdot 10^{-4}, 5.8311 \cdot 10^{-17}\}$  and thus suggests to preserve the  $r = 3$  first columns of  $\mathbf{Y}$  and  $\mathbf{X}$ , as in (10). After projection, this leads to a minimal order realization which related transfer function exactly recovers the original  $\mathbf{H}$ , with McMillan degree of  $v = 2$  and associated realization  $r = 3$ . In addition, computing the singularities of the associated pencil  $(\mathbb{M}, \mathbb{L})$  gives  $\{-1, \infty, \infty\}$ , being exactly the one of the original model  $\mathbf{H}$ . The singularity in  $-1$  is related to the rational part of  $\mathbf{H}$ ,  $1/(s + 1)$  (finite dynamic mode). The two singularities in  $\infty$  are related to the impulsive (polynomial part) and non-dynamic (direct feed-through term) modes.

**Example 2** (Interpolation in the sampled-time). Let us consider the discrete-time model  $\mathbf{H}(z) = z/(z - 1/2)$ , with sampling period  $h = 1$  second. We evaluate the function on the unit circle centered in zero. Then, by choosing  $\lambda_i = \{e^{-i0.1h}, e^{i0.1h}, e^{-i2h}, e^{i2h}\}$ ,  $\mu_j = \{e^{-ih}, e^{ih}, e^{-i3h}, e^{i3h}\}$  and tangential directions  $\mathbf{r}_i = \mathbf{l}_j = 1$  for  $i, j = 1, \dots, 4 = \bar{n} = \underline{n}$  ( $N = 8$ ), one obtains  $\mathbf{w}_i$  and  $\mathbf{v}_j$ . By construction, the Loewner matrices of dimension  $4 \times 4$  contain complex entries. As data are provided in complex conjugate form, one may work with real arithmetic by projecting (see §2.5.4 Karachalios et al., 2020a for details).

By then solving (5), one readily obtains  $\mathbb{L}$  and  $\mathbb{M}$  and the associated 4-th order realization  $\mathcal{S}_N : (-\mathbb{L}, -\mathbb{M}, \mathbf{V}, \mathbf{W}, \mathbf{0})$ . Applying the rank revealing factorization (9) and (10), one obtains the McMillan degree  $v = \text{rank}(\mathbb{L}) = 1$  and  $r = 2$ . This suggests a constant term. By applying the procedure in Gosea et al. (2020), the direct term is reconstructed by the infinite eigenvalue computation of  $(\mathbb{M}, \mathbb{L})$  pencil. In this case one finds  $D = 1$ . By removing it from the data and re-computing the Loewner procedure, one finds  $v = r = 1$  and the sampled realization  $(\mathbf{E}_1, \mathbf{A}_1, \mathbf{B}_1, \mathbf{C}_1, \mathbf{D}_1) = (2.897, 1.448, -0.9632, -1.504, 1)$ , with transfer function  $\mathbf{H}_1 = (z - 1.665 \times 10^{-16})/(z - 0.5)$ , recovering almost perfectly  $\mathbf{H}$ .

## 2.3 Generalizations to parametric linear systems

The Loewner framework has been extended to parametric **LTI (pLTI)** systems, first in Antoulas et al. (2012) and in a more detailed manner in Ionita and Antoulas (2014).<sup>5</sup> In parametric model approximation and reduction, the aim is to construct reduced-order models that match the response of the original model / data, along the dynamical parameter  $\xi$  (usually complex) and along parameter  $\rho$  (real-valued). In what follows we will only show how the two variable case works, *i.e.* with one single parameter  $\rho \in \mathbb{R}$  (for further extensions, see Ionita and Antoulas, 2014). We construct models which are reduced both with respect to the complex variable (frequency) and to the real one (parameter). In this configuration, let us consider such a  $m$  input  $p$  output  $\rho$ -parametrized dynamical system described by a  $n$ -th order differential algebraic equation (**DAE**) model denoted  $\mathcal{S}(\rho) : (\mathbf{E}(\rho), \mathbf{A}(\rho), \mathbf{B}(\rho), \mathbf{C}(\rho), \mathbf{0})$  given as  $\mathbf{E}(\rho)\dot{\mathbf{x}}(t) = \mathbf{A}(\rho)\mathbf{x}(t) + \mathbf{B}(\rho)\mathbf{u}(t)$ ,  $\mathbf{y}(t) = \mathbf{C}(\rho)\mathbf{x}(t)$  where  $\mathbf{E}(\rho), \mathbf{A}(\rho) \in \mathbb{R}^{n \times n}$ ,  $\mathbf{B}(\rho) \in \mathbb{R}^{n \times m}$ ,  $\mathbf{C}(\rho) \in \mathbb{R}^{p \times n}$ ,  $\rho \in \mathbb{R}$ , with associated transfer function  $\mathbf{H} : (\mathbb{C} \times \mathbb{R}) \setminus \Lambda(\mathbf{A}(\rho), \mathbf{E}(\rho)) \rightarrow \mathbb{C}^{p \times m}$  given for  $\Phi(\xi, \rho) = (\xi \mathbf{E}(\rho) - \mathbf{A}(\rho))^{-1} \in \mathbb{C}^{n \times n}$ , as:

$$\mathbf{H}(\xi, \rho) = \mathbf{C}(\rho)\Phi(\xi, \rho)\mathbf{B}(\rho). \quad (11)$$

---

<sup>5</sup> The approach developed in Ionita and Antoulas (2014) interpolates more frequencies and parameter combinations than the approach derived in Antoulas et al. (2012). This latter interpolates an extended Loewner matrix instead and leads to the coefficients of a rational and polynomial function given in the Barycentric form.

As for the Loewner case, let us assume that function (11) can be expressed using the distinct Lagrange support points  $\lambda_i$  and  $\pi_j$ , as (for  $\alpha_{ij} \neq 0$ )

$$\mathbf{H}(\xi, \rho) = \frac{\sum_{i=1}^{n+1} \sum_{j=1}^{m+1} \beta_{ij} \mathbf{q}_{ij}(\xi, \rho)}{\sum_{i=1}^{n+1} \sum_{j=1}^{m+1} \alpha_{ij} \mathbf{q}_{ij}(\xi, \rho)} \text{ where } \mathbf{q}_{ij}(\xi, \rho) = \frac{1}{(\xi - \lambda_i)(\rho - \pi_j)}. \quad (12)$$

Note that the above structure is not restrictive at all since it provides a parametrization as a function of support points (see Nakatsukasa et al., 2018; Berrut and Trefethen, 2006). Computation of the approximant is done in a similar way as for the non-parametric rational case: one seeks the  $\beta_{ij}$  and  $\alpha_{ij}$  of the rational barycentric formula (12). Assuming that  $\mathbf{H}(\xi, \rho)$  is sampled along the dynamical parameter  $\xi$  and the parametric one  $\rho$  as

$$\{z_k\}_{k=1}^N = \{\lambda_i\}_{i=1}^{\bar{n}} \cup \{\mu_j\}_{j=1}^{\underline{n}} \text{ and } \{p_l\}_{l=1}^M = \{\pi_i\}_{i=1}^{\bar{m}} \cup \{\nu_j\}_{j=1}^{\underline{m}}, \quad (13)$$

leading to  $\mathbf{H}(z_k, p_l) = \Phi_{k,l}$ . Thus the measurement matrix reads

$$\Phi = \begin{bmatrix} \Phi_{(11)} & \Phi_{(12)} \\ \Phi_{(21)} & \Phi_{(22)} \end{bmatrix} \in \mathbb{C}^{N \times M}, \quad (14)$$

where  $\Phi_{(11)} = \Phi_{1, \dots, \bar{n}/1, \dots, \bar{m}} \in \mathbb{C}^{\bar{n} \times \bar{m}}$ ,  $\Phi_{(12)} = \Phi_{1, \dots, \bar{n}/1, \dots, \underline{m}} \in \mathbb{C}^{\bar{n} \times \underline{m}}$ ,  $\Phi_{(21)} = \Phi_{1, \dots, \underline{n}/1, \dots, \bar{m}} \in \mathbb{C}^{\underline{n} \times \bar{m}}$ , and  $\Phi_{(22)} = \Phi_{1, \dots, \underline{n}/1, \dots, \underline{m}} \in \mathbb{C}^{\underline{n} \times \underline{m}}$ . The rows correspond to frozen values of  $z_k$  related to the dynamical (complex)  $\xi$  parameter. The columns correspond to frozen  $p_l$  values related to the (real)  $\rho$  parameter. Similarly to the non-parametric case mentioned in Section 2.2, one may construct the following one variable Loewner matrices: (i)  $\mathbb{L}_2 \in \mathbb{C}^{\underline{n}\bar{m} \times \bar{n}\bar{m}}$  associated to  $\Phi_{(11)}$  along  $\lambda_i \cup \pi_j$ , (ii)  $\mathbb{L}_{\lambda_i} \in \mathbb{C}^{\underline{n} \times \bar{m}}$  associated to the  $i$ -th row of  $[\Phi_{(11)}, \Phi_{(12)}]$  along  $p_l$  and (iii)  $\mathbb{L}_{\pi_j} \in \mathbb{C}^{\bar{n} \times \bar{n}}$  associated to the  $j$ -th column of  $[\Phi_{(11)}^H, \Phi_{(21)}^H]^H$  along  $z_k$ .

Then the global two dimensional Loewner matrix  $\widehat{\mathbb{L}}_2 = [\mathbb{L}_{\lambda}^H \mathbb{L}_{\pi}^H \mathbb{L}_2^H]^H \in \mathbb{C}^{(\bar{n}\bar{m} + \underline{n}\bar{m} + \underline{n}\underline{m}) \times (\bar{n}\bar{m})}$ , where  $\mathbb{L}_{\lambda} = [(\mathbf{e}_1^T \otimes \mathbb{L}_{\lambda_1})^H \dots (\mathbf{e}_n^T \otimes \mathbb{L}_{\lambda_{\bar{n}}})^H]^H$  and  $\mathbb{L}_{\pi} = [(\mathbb{L}_{\pi_1} \otimes \mathbf{e}_1^T)^H \dots (\mathbb{L}_{\pi_{\bar{n}}} \otimes \mathbf{e}_{\bar{n}}^T)^H]^H$ .

As in the non-parametric case, one important step is the determination of the minimal rational orders  $n$  and  $m$  in (12) hidden in the data collection. This is computed by evaluating the null-space of the single variable Loewner matrices combinations

$$r = \max_l \operatorname{rank} \mathbb{L}_{p_l} \text{ and } q = \max_k \operatorname{rank} \mathbb{L}_{z_k}, \quad (15)$$

where  $\mathbb{L}_{p_l}$  and  $\mathbb{L}_{z_k}$  are the one dimensional Loewner matrices associated to the  $k$ -th row and  $l$ -th column of  $\Phi$ , respectively. Then, one can simply set  $(\bar{n}, \bar{m}) = (r+1, q+1)$ , partition the data (13)-(14), and reconstruct  $\widehat{\mathbb{L}}_2$ . The two dimensional Loewner matrices ensure  $\operatorname{rank} \widehat{\mathbb{L}}_2 = \operatorname{rank} \mathbb{L}_2 = \bar{n}\bar{m} - (\bar{n}-r)(\bar{m}-q) = \bar{n}\bar{m} - 1$ . The coefficients  $\alpha_{ij}$  and  $\beta_{ij}$  of the two variables barycentric transfer

function interpolating the data, are obtained by computing the null-space of  $\widehat{\mathbb{L}}_2$  as  $\mathbf{c} = \ker \widehat{\mathbb{L}}_2$  where  $\mathbf{c} \in \mathbb{C}^{(r+1) \times (q+1)}$ . Note that it is usually preferred to work with real arithmetic, *e.g.* for model time domain simulation or control design and analysis. In that case  $z_k$  are compiled in a closed conjugate form and support points are doubled (refer to §A.2 of Ionita and Antoulas, 2014 for detailed exposition). Note also that a trade-off between accuracy and complexity with both the frequency and the parameter variables can be obtained by decreasing the order  $r$  and  $q$  below the one given by (15).

Following the barycentric formulae, and Ionita and Antoulas (2014); Antoulas et al. (2012), one may reconstruct the associated multi-valued transfer function  $\mathbf{H}_{r,q} : (\mathbb{C} \times \mathbb{R}) \times \Lambda_{\mathbf{H}_{r,q}} \rightarrow \mathbb{C}^{p \times m}$  as follows (where  $\Phi(\xi, \rho) \in \mathbb{C}^{N_{r,q} \times N_{r,q}}$ ,  $N_{r,q} = r + 2q + 2$ )

$$\mathbf{H}_{r,q}(\xi, \rho) = \mathbf{C}\Phi^{-1}(\xi, \rho)\mathbf{B}$$

$$\text{where } \Phi(\xi, \rho) = \begin{bmatrix} \mathbf{J}_{\lambda,r}(\xi) & \mathbf{0} & \mathbf{0} \\ \mathbb{A} & \mathbf{J}_{\pi,q}^T(\rho) & \mathbf{0} \\ \mathbb{B} & \mathbf{0} & [\mathbf{J}_{\pi,q}(\rho), \boldsymbol{\tau}] \end{bmatrix}, \quad (16)$$

with  $\mathbf{B} = [\mathbf{0}, \boldsymbol{\tau}, \mathbf{0}]^T \in \mathbb{R}^{N_{r,q}}$  and  $\mathbf{C} = [0, \dots, 0, -1] \in \mathbb{R}^{N_{r,q}}$ . Moreover, the following holds for  $k = 1, \dots, r$ ,  $l = 1, \dots, q$  and  $\mathbf{w} = \text{vect}(\Phi_{(11)})$ :  $\mathbb{A}_{:,k} = [\mathbf{c}_{k,1}^H \dots \mathbf{c}_{k,q+1}^H]^H$ ,  $\mathbb{B}_{:,k} = [(\mathbf{c}_{k,1}\mathbf{w}_{k,1})^H \dots (\mathbf{c}_{k,q+1}\mathbf{w}_{k,q+1})^H]^H$  and  $\boldsymbol{\tau}_k^{-1} = \prod_{l=1, l \neq k}^{q+1} (\pi_k - \pi_l)$  and with

$$\mathbf{J}_{\eta,t}(x) = \begin{bmatrix} x - \eta_1 & \eta_2 - x & & \\ \vdots & & \ddots & \\ x - \eta_1 & & & \eta_{t+1} - x \end{bmatrix} \in \mathbb{C}^{t \times (t+1)}. \quad (17)$$

Notice that (16) depends only on the extended Loewner matrix null-space  $\mathbf{c}$ , support points  $\{\lambda_i\}_{i=1}^{r+1}$ ,  $\{\pi_j\}_{j=1}^{q+1}$  and the response data matrix  $\{\Phi_{(11)}\}_{i,j=1}^{r+1, q+1}$ .

**Remark 3** (Minimal realization in the multi-parametric case). Realization (16) is no longer identical to the one in the single variable case as the resolvent  $\Phi(\xi, \rho)$  includes both the dynamic and parametric variables, leading instead to an order  $N_{r,q}$  of  $r$ . Finding a minimal order realization is still an open problem.

**Remark 4 (SIMO, MISO, and MIMO cases).** Both **SIMO** and **MISO** cases can be addressed by tangential interpolating the data instead of the scalar (see §A.1 of Ionita and Antoulas, 2014 for details). Extension to the **MIMO** case is not solved yet. The tangential approach used in the non-parametric case and in most of multi-port interpolation frameworks (Gallivan et al., 2004) is not applicable as is. An alternative approach is presented in Lefteriu et al. (2011) but which “only” interpolates  $\Phi_{(11)}$ , forgetting  $\Phi_{(12)}$  and  $\Phi_{(21)}$ .

**Example 3** (Reynolds parameter dependent linearized Navier-Stokes model). Let us consider a two-dimensional open square cavity fluid-flow problem where air flows from left to right for three different Reynolds numbers  $Re = 4000$ ,  $5250$ , or  $6000$ . Such a configuration, illustrated on Fig. 1 (top right), is described in Barbagallo et al. (2008) and in Poussot-Vassal and Sipp (2015). For simulation, Navier-Stokes equations are used along a mesh composed of  $193,874$  triangles, corresponding to  $n = 680,974$  degrees of freedom for the velocity variables along the  $x$  and  $y$  axis. After linearization around three fixed points for Reynolds numbers, and discretization along the flow axis,  $\{\mathbf{H}_l\}_{l=1}^3$  can be described as a DAE realization of order  $n = 680,974$  where the input  $\mathbf{u}(t)$  is the vertical pressure actuator located upstream of the cavity and the output  $\mathbf{y}(t)$  is a shear stress sensor, located downstream of the cavity. A set of continuous-time  $n$ -th order realization  $\mathcal{S}_l : (\mathbf{E}, \mathbf{A}_l, \mathbf{B}, \mathbf{C}, \mathbf{0})$  are obtained. In Poussot-Vassal and Sipp (2015), the IRKA approach (Gugercin et al., 2008) is used to sequentially approximate each realization with a low dimensional one. The interpolation along the parameter is done in a second step by interpolating each coefficients in the canonical basis of the obtained reduced models. Here instead, the parametric Loewner framework is applied. The frequency response of each configuration along  $\{z_k\}_{k=1}^N = z_0 \cup \{\iota\omega_k, -\iota\omega_k\}_{k=1}^{100}$ , where  $z_0 \in \mathbb{R}_+$  and  $\omega_k$  logarithmically-spaced frequencies. Then, twenty intermediate configurations between each Reynolds numbers  $Re = 4000, 5250, 6000$  are constructed by linear interpolation. We obtain  $\{z_k\}_{k=1}^{N=201}$ ,  $\{p_l\}_{l=1}^{N=41}$  and thus  $\Phi \in \mathbb{C}^{201 \times 41}$ . Our objective is to come up with a parametrized linear model that is able to faithfully reproduce the original transfer function data on a particular range of frequencies as well as on a parameter range.<sup>6</sup>

Fig. 1 (top left) depicts two types of singular values. The singular values drop indicates reduction orders  $r = 30$  and  $q = 20$  for building the two dimensional Loewner matrix. As a real valued rational function is preferred rather than a complex one, the twice more support points are considered and realization size is increased. The reduced linear parametric model is sampled over the same frequency and parameter range as before. When comparing to the original samples on Fig. 1 (bottom), the overall result is satisfactory, with a model of complexity  $r = 60$  (instead of  $n = 680,974$ ) and  $q = 20$  (instead of a collection).

## 2.4 Generalization to modeling from time-domain data

For a linear, time-invariant SISO system, let the impulse response be denoted with:  $\mathbf{h} = \{\dots, \mathbf{h}_{-2}, \mathbf{h}_{-1}, \mathbf{h}_0, \mathbf{h}_1, \mathbf{h}_2, \dots\}$ . Here we restrict our attention to causal systems:  $\mathbf{h}_k = 0$ ,  $k < 0$ ; furthermore it is assumed that  $\mathbf{u}(t) = 0$ ,  $t < 0$ . Hence, one can write that

$$\mathbf{y}(t) = \mathbf{h}_0 \mathbf{u}(t) + \mathbf{h}_1 \mathbf{u}(t-1) + \dots + \mathbf{h}_k \mathbf{u}(t-k) + \dots, \quad t \in \mathbb{Z}_+. \quad (18)$$

<sup>6</sup> Additional details and the data are available at [https://morwiki.mpi-magdeburg.mpg.de/morwiki/index.php/Fluid\\_Flow\\_Linearized\\_Open\\_Cavity\\_Model](https://morwiki.mpi-magdeburg.mpg.de/morwiki/index.php/Fluid_Flow_Linearized_Open_Cavity_Model).

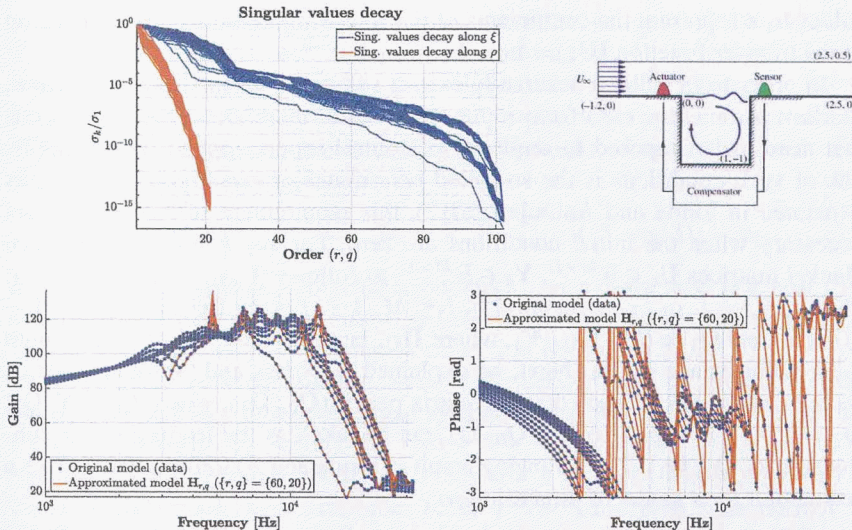


**FIGURE 1** Top left: singular values drop of the one variable Loewner matrices (15). Top right: schematic view of the geometry (with illustration of the control structure used in Poussot-Vassal et al., 2018). Bottom frames: frequency response gain and phase of the original sampled data (blue dots) and resulting parametric model  $H_{60,20}$  for some parametric values (solid orange lines).

In the formulation above,  $\mathbf{h}_j$  denotes the  $j^{\text{th}}$  Markov parameter of the underlying system. In the time domain, the data are samples of input and output signals

$$\mathbf{u}_N = [\mathbf{u}_0, \dots, \mathbf{u}_{N-1}], \quad \mathbf{y}_N = [\mathbf{y}_0, \dots, \mathbf{y}_{N-1}], \quad (19)$$

where, for simplicity, we have used the shortened expressions  $\mathbf{u}_k := \mathbf{u}(k)$  and  $\mathbf{y}_k := \mathbf{y}(k)$ . The system identification problem consists in recovering a discrete-time linear time invariant system compatible with the data in (19). We seek a minimal realization ( $\mathbf{E}, \mathbf{A}, \mathbf{B}, \mathbf{C}, \mathbf{D}$ ):

$$\mathcal{S}_D : \mathbf{E} \mathbf{x}(t+1) = \mathbf{A} \mathbf{x}(t) + \mathbf{B} \mathbf{u}(t), \quad \mathbf{y}(t) = \mathbf{C} \mathbf{x}(t) + \mathbf{D} \mathbf{u}(t), \quad (20)$$

where  $\mathbf{E}, \mathbf{A} \in \mathbb{R}^{n \times n}$ ,  $\mathbf{B}, \mathbf{C}^T \in \mathbb{R}^{n \times 1}$ ,  $\mathbf{D} \in \mathbb{R}$ , with the transfer function

$$\mathbf{H}(z) = \mathbf{C}(z\mathbf{E} - \mathbf{A})^{-1}\mathbf{B} + \mathbf{D} = \frac{b_m z^m + \dots + b_1 z + b_0}{z^n + \dots + a_1 z + a_0}, \quad m \leq n. \quad (21)$$

The Markov parameters in (18) can be explicitly written in terms of matrices from the realization in (20), as follows:

$$\mathbf{h}_0 = \mathbf{D}, \quad \mathbf{h}_k = \mathbf{C}\mathbf{A}^{k-1}\mathbf{B}, \quad \forall k \geq 1. \quad (22)$$

Moreover, another interpretation of Markov parameters is that they encode the behavior of the transfer function in  $\mathbf{H}(z)$  in (21) at  $z = \infty$ . More precisely, the

values  $\mathbf{h}_k$ 's represent the coefficients of the following Laurent series expansion of the transfer function  $\mathbf{H}(z) = \mathbf{h}_0 + \mathbf{h}_1 z^{-1} + \mathbf{h}_2 z^{-2} + \cdots + \mathbf{h}_k z^{-k} + \cdots$ .

In order to be able to accurately extract system invariants (poles, residues, Markov parameters, etc.) from input-output data, there are certain conditions that need to be imposed to sequence of control inputs applied. For example, one of such conditions is the so-called *persistence of excitation*. However, as explained in Ionita and Antoulas (2012), this requirement of the input is not necessary when the initial conditions are zero. For any  $k \geq 0$ , we introduce Hankel matrices  $\mathbf{U}_k \in \mathbb{R}^{M \times L}$ ,  $\mathbf{Y}_k \in \mathbb{R}^{M \times L}$ , as follows  $(\mathbf{U}_k)_{i,j} = u_{k+i-1,k+j-1}$ ,  $(\mathbf{Y}_k)_{i,j} = y_{k+i-1,k+j-1}$ , for all  $1 \leq i \leq M$ ,  $1 \leq j \leq L$ . Let also  $\mathbf{Q}_0 = (\mathbf{I} - \mathbf{\Pi}_{\mathbf{U}_0})\mathbf{Y}_0$  and  $\mathbf{Q}_1 = (\mathbf{I} - \mathbf{\Pi}_{\mathbf{U}_0})\mathbf{Y}_1$ , where  $\mathbf{\Pi}_{\mathbf{U}_0}$  be the orthogonal projection onto the column space of  $\mathbf{U}_0$ . Next, as explained in Ionita and Antoulas (2012), there exists matrix  $\mathbf{Y}$ , such that the matrix pencil  $(\widehat{\mathbf{Q}}_0, \widehat{\mathbf{Q}}_1)$ , where  $\widehat{\mathbf{Q}}_0 = \mathbf{Y}^* \mathbf{Q}_0$ ,  $\widehat{\mathbf{Q}}_1 = \mathbf{Y}^* \mathbf{Q}_1$ , is regular (often  $\widehat{\mathbf{Q}}_0, \widehat{\mathbf{Q}}_1$  can be taken as the leading  $n \times n$  submatrices of  $\mathbf{Q}_0, \mathbf{Q}_1$ ). The following result in Ionita and Antoulas (2012) gives a realization for a model of dimension  $n$ :

**Theorem 1.** *For zero initial conditions, the system has a minimal realization*

$$\widetilde{\mathbf{E}} = \widehat{\mathbf{Q}}_0, \quad \widetilde{\mathbf{A}} = \widehat{\mathbf{Q}}_1, \quad \widetilde{\mathbf{B}} = \mathbf{q}_0, \quad \widetilde{\mathbf{C}} = [\mathbf{h}_1, \dots, \mathbf{h}_n], \quad \widetilde{\mathbf{D}} = \mathbf{h}_0,$$

where  $\mathbf{q}_0$  is the first column of  $\widehat{\mathbf{Q}}_0$  and the Markov parameters  $\mathbf{h}_j$ 's are obtained by solving the following linear system of equations

$$\begin{bmatrix} \mathbf{u}_0 & & & \\ \mathbf{u}_1 & \mathbf{u}_0 & & \\ \vdots & \ddots & \ddots & \\ \mathbf{u}_n & \cdots & \mathbf{u}_1 & \mathbf{u}_0 \end{bmatrix} \begin{bmatrix} \mathbf{h}_0 \\ \mathbf{h}_1 \\ \vdots \\ \mathbf{h}_n \end{bmatrix} = \begin{bmatrix} \mathbf{y}_0 \\ \mathbf{y}_1 \\ \vdots \\ \mathbf{y}_n \end{bmatrix}. \quad (23)$$

The Markov parameters can hence be computed for any input  $\mathbf{u}$ . The result in Theorem 1 can indeed be further specialized for the case of  $\mathbf{u} = [1, 0, \dots, 0]$ . Hence, when the input is an impulse, the output is a finite sequence of Markov parameters, *i.e.*,  $\mathbf{y} = [\mathbf{h}_0, \mathbf{h}_1, \dots, \mathbf{h}_{N-1}]$ . The realization in Theorem 1 is hence appropriately modified; let  $\tilde{\mathcal{S}}_n$  be the new realization given by

$$\widetilde{\mathbf{E}} = \begin{bmatrix} \mathbf{h}_1 & \mathbf{h}_2 & \cdots & \mathbf{h}_n \\ \mathbf{h}_2 & \mathbf{h}_3 & \cdots & \mathbf{h}_{n+1} \\ \vdots & \vdots & \ddots & \vdots \\ \mathbf{h}_n & \mathbf{h}_{n+1} & \cdots & \mathbf{h}_{2n-1} \end{bmatrix}, \quad \widetilde{\mathbf{A}} = \begin{bmatrix} \mathbf{h}_2 & \mathbf{h}_3 & \cdots & \mathbf{h}_{n+1} \\ \mathbf{h}_3 & \mathbf{h}_4 & \cdots & \mathbf{h}_{n+2} \\ \vdots & \vdots & \ddots & \vdots \\ \mathbf{h}_{n+1} & \mathbf{h}_{n+2} & \cdots & \mathbf{h}_{2n} \end{bmatrix}, \quad (24)$$

$$\widetilde{\mathbf{C}} = [\mathbf{h}_1, \mathbf{h}_2, \dots, \mathbf{h}_n], \quad \widetilde{\mathbf{B}} = \widetilde{\mathbf{C}}^T, \quad \widetilde{\mathbf{D}} = \mathbf{h}_0.$$

As in Section 2.2, we could further reduce the dimension of the fitted model in (24) by means of projection (compressing the realization of order  $n$  to one of

order  $r$  by means of orthogonal matrices computed using the **SVD** Antoulas, 2005, chap. 3). In this case, we enforce approximation, *i.e.* by fitting a model which approximately explains the data. Hence, let  $\mathbf{Y} \in \mathbb{R}^{n \times r}$  (resp.  $\mathbf{X} \in \mathbb{R}^{n \times r}$ ) be the matrix containing the first  $r$  left and respectively, right singular vectors of the Hankel matrix denoted in (24) by  $\tilde{\mathbf{E}}$ . The reduced-order realization  $\tilde{\mathcal{S}}_r : (\tilde{\mathbf{E}}_r, \tilde{\mathbf{A}}_r, \tilde{\mathbf{B}}_r, \tilde{\mathbf{C}}_r, \mathbf{0})$  is computed:

$$\tilde{\mathbf{E}}_r = \mathbf{Y}^T \tilde{\mathbf{E}} \mathbf{X}, \tilde{\mathbf{A}}_r = \mathbf{Y}^T \tilde{\mathbf{A}} \mathbf{X}, \tilde{\mathbf{B}}_r = \mathbf{Y}^T \tilde{\mathbf{B}}, \tilde{\mathbf{C}}_r = \tilde{\mathbf{C}} \mathbf{X}, \text{ and } \tilde{\mathbf{D}}_r = \mathbf{h}_0. \quad (25)$$

**Example 4** (A structural mechanics model). As a numerical test case, we consider the model of a building (the Los Angeles University Hospital) from the NICONET benchmark examples collection (Niconet, 2002). The original model is a second-order linear system of dimension  $n_0 = 24$ . It can be written equivalently as a first-order linear system of dimension  $n = 48$ . We modify the original model by scaling the vector  $\mathbf{B} \in \mathbb{R}^{48}$  with  $10^4$ . Then, the original continuous-time LTI model of dimension  $n = 48$  is discretized using a classical Backward Euler first order scheme. The simulation time horizon is  $[0, 5]$ s, while the time step is  $\Delta t = 4 \cdot 10^{-3}$ . The control input is chosen to be  $u(t) = \frac{1}{10}(\cos(50t) + 2\cos(20t) + 3\cos(10t))$ . Hence, by means of this time-domain simulation, we collect  $N = 2001$  measurements of the discretized input and output, *i.e.*, as in (19). These values are depicted in the left pane of Fig. 2. The Markov parameters are extracted by following the approach in Ionita and Antoulas (2012), and are depicted in the right pane of Fig. 2 (there, the magnitude of the error between the true Markov parameters and the estimated ones is shown in orange).

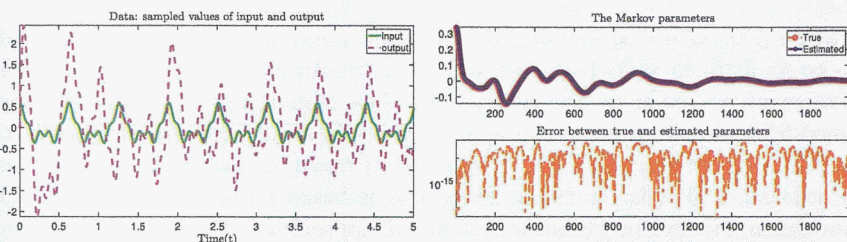


**FIGURE 2** Samples of the input and output signals (left) and the true and recovered Markov parameters (right).

Next, form a  $1000 \times 1000$  Hankel matrix as in (24). The decay of its singular values is displayed in the left pane of Fig. 3. Then, choose the truncation order  $r = 20$ , and construct a realization of order  $r$  as presented in (25). Finally, convert this discrete-time model back to the continuous time, and compare the frequency response of the original model of order  $n$ , with that of the reduced one of order  $r$  (on a range of 500 frequency points in the interval  $[10^0, 10^2]$ ). The results (frequency responses and the approximation error) are presented in the right pane of Fig. 3. Indeed, the model is well approximated by means of the proposed method.

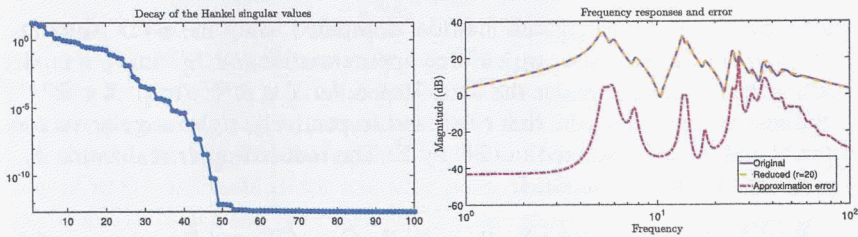


**FIGURE 3** Decay of the Hankel singular values (left) and frequency responses computations: original, reduced and the approximation error (right).

**Remark 5.** As shown in this experiment, the estimated Markov parameters illustrated in Fig. 2 match the original ones quite well (up to  $O(10^{-14})$  errors). This accurate matching is explained by the fact that the input and output were assumed to be measured without noise. However, in practical applications such measurements could be indeed perturbed by various exogenous sources. An exact quantification of how the noise affects the Markov parameter estimation will be studied in future works specifically for the method presented here (a generic analysis is readily available in Ljung, 1987, Chapter 8).

## 2.5 Extensions to nonlinear systems

Consider a nonlinear system described by the following equations  $\mathcal{S}_N$

$$\dot{\mathbf{x}}(t) = \mathbf{f}(\mathbf{x}(t)) + \mathbf{g}(\mathbf{x}(t))\mathbf{u}(t), \quad \mathbf{y}(t) = \mathbf{C}\mathbf{x}(t), \quad (26)$$

where  $t \geq 0$ ,  $\mathbf{x}(0) = \mathbf{x}_0$  and the nonlinear functions  $\mathbf{f}, \mathbf{g} : \mathbb{R}^n \rightarrow \mathbb{R}^n$  are assumed to be analytic in  $\mathbf{x}(t)$ . Here, we will focus on an extension of the Loewner framework to reducing bilinear systems. The motivation for this is that any smooth, nonlinear system with analytical nonlinearities can be approximated by a bilinear system. This is accomplished by means of Carleman linearization (Carleman, 1932; Rugh, 1981). Since this is based on Taylor expansion and truncation, the resulting bilinear system will approximate the original nonlinear system depending on the number of terms kept in the expansion. We proceed by writing the truncated *Taylor series* for the non-linear functions  $\mathbf{f}$  and  $\mathbf{g}$ , i.e.

$$\begin{cases} \mathbf{f}(\mathbf{x}) \approx \sum_{k=0}^N \mathbf{F}_k \mathbf{x}^{(N)} = \mathbf{F}_0 + \mathbf{F}_1 \mathbf{x} + \mathbf{F}_2 \mathbf{x}^{(2)} + \dots + \mathbf{F}_N \mathbf{x}^{(N)}, \\ \mathbf{g}(\mathbf{x}) \approx \sum_{k=0}^{N-1} \mathbf{G}_k \mathbf{x}^{(k)} = \mathbf{G}_0 + \mathbf{G}_1 \mathbf{x} + \dots + \mathbf{G}_{N-1} \mathbf{x}^{(N-1)}, \end{cases} \quad (27)$$

where  $\mathbf{F}_0, \mathbf{G}_0 \in \mathbb{R}^{n \times 1}$ ,  $\mathbf{F}_j, \mathbf{G}_j \in \mathbb{R}^{n^j \times n^j}$ ,  $j \geq 1$  and  $N$  is the truncation index. Here, the term  $\mathbf{F}_0$  is usually chosen to be  $\mathbf{0}$  in the case of non-existing forcing terms (if indeed is non-zero, it can be incorporated in the state vector by means of shifting). Additionally,  $\mathbf{F}_1, \mathbf{G}_1$  denote the Jacobian matrices of  $\mathbf{f}$  and  $\mathbf{g}$ , respectively, and  $\mathbf{F}_k, \mathbf{G}_k$  denote the matrices of higher derivatives. Moreover  $\mathbf{x}^{(k)}$

denotes the Kronecker product of the state variable  $\mathbf{x}$  with itself ( $k$  times). Then, introduce a new state variable

$$\mathbf{x}^{\otimes}(t) = \begin{bmatrix} \mathbf{x}(t) & \mathbf{x}^{(2)}(t) & \dots & \mathbf{x}^{(N)}(t) \end{bmatrix}^T \in \mathbb{R}^{n^{(N)}},$$

where  $n^{(N)} = n + n^2 + \dots + n^N = \frac{n^{N+1}-n}{n-1}$ . This is obtained by concatenating all higher powers of vector  $\mathbf{x}$  (up to  $N$ ). In this way, by computing derivatives of  $\mathbf{x}^{(k)}$ , we obtain a bilinear system with the following realization

$$\dot{\mathbf{x}}^{\otimes}(t) \approx \mathbf{A}^{\otimes}\mathbf{x}^{\otimes}(t) + \mathbf{N}^{\otimes}\mathbf{x}^{\otimes}(t)\mathbf{u}(t) + \mathbf{B}^{\otimes}\mathbf{u}(t), \quad \mathbf{y} = \mathbf{C}^{\otimes}\mathbf{x}^{\otimes}(t), \quad (28)$$

where  $\mathbf{x}^{\otimes}(0) = \mathbf{0}$  and the matrices  $\mathbf{A}^{\otimes}, \mathbf{N}^{\otimes} \in \mathbb{R}^{n^{(N)} \times n^{(N)}}, \mathbf{B}^{\otimes}, (\mathbf{C}^{\otimes})^T \in \mathbb{R}^{n^{(N)}}$  are as in (Gosea, 2017, Section 2.1.1). In what follows, we employ a more generic definition of bilinear systems  $\mathcal{S}_B : (\mathbf{C}, \mathbf{E}, \mathbf{A}, \mathbf{N}, \mathbf{B})$ , characterized by:

$$\dot{\mathbf{E}}\mathbf{x}(t) = \mathbf{A}\mathbf{x}(t) + \mathbf{N}\mathbf{x}(t)\mathbf{u}(t) + \mathbf{B}\mathbf{u}(t), \quad \mathbf{y}(t) = \mathbf{C}\mathbf{x}(t), \quad (29)$$

where  $\mathbf{E}, \mathbf{A}, \mathbf{N} \in \mathbb{R}^{n \times n}, \mathbf{B} \in \mathbb{R}^{n \times m}, \mathbf{C} \in \mathbb{R}^{p \times n}$ , and  $\mathbf{x} \in \mathbb{R}^n, \mathbf{u}, \mathbf{y} \in \mathbb{R}$ . The matrix  $\mathbf{E}$  is assumed to be non-singular. Also, for simplicity of exposition, we will discuss only the **SISO** case. More details on bilinear system model order reduction can be found in Breiten and Damm (2010); Benner and Breiten (2012); Flagg and Gugercin (2015). Bilinear systems as in (29) are equivalent to an infinite collection of coupled linear time-varying systems:

$$\dot{\mathbf{E}}\mathbf{x}_1(t) = \mathbf{A}\mathbf{x}_1(t) + \mathbf{B}\mathbf{u}(t), \quad \dot{\mathbf{E}}\mathbf{x}_i(t) = \mathbf{A}\mathbf{x}_i(t) + \mathbf{N}\mathbf{x}_{i-1}(t)\mathbf{u}(t), \quad i \geq 2. \quad (30)$$

The time-varying factor appears only in the matrices that scale the control input  $\mathbf{u}(t)$  at each level  $i \geq 2$ . Based on (30), the solution of (29) is decomposed as  $\mathbf{x}(t) = \sum_{i=1}^{\infty} \mathbf{x}_i(t)$ . Furthermore, the input-output representation of the bilinear system  $\mathcal{S}_B$  can be expressed in terms of the *Volterra series representation* (Rugh, 1981; Flagg and Gugercin, 2015). Moreover, considering  $\mathbf{x}_{i-1}(t)$  in the  $i^{\text{th}}$  equation as a pseudo-input for  $i = 1, 2, \dots$ , the frequency-domain behavior is described by a series of generalized transfer functions as given also in Rugh (1981); Flagg and Gugercin (2015); Antoulas et al. (2016a):

$$\mathbf{H}_i(s_1, s_2, \dots, s_i) = \mathbf{C}\Phi(s_1)\mathbf{N}\Phi(s_2)\mathbf{N} \cdots \mathbf{N}\Phi(s_i)\mathbf{B}, \quad (31)$$

where the resolvent of the pencil  $(\mathbf{A}, \mathbf{E})$  is denoted by  $\Phi(\xi) = (\xi\mathbf{E} - \mathbf{A})^{-1}$ . The characterization of bilinear systems by means of the rational functions in (31) suggests that reduction of such systems can be performed by means of the Loewner framework. In what follows, we will review some highlights of the procedure originally presented in Antoulas et al. (2016a). We use the concept of multi-tuples, composed of multiple interpolation points corresponding to evaluations of the transfer functions in (31). For simplicity, we will assume that

one set of right multi-tuples  $\lambda$ , and one set of left multi-tuples  $\mu$  with the same number of interpolation points (denoted with  $k$ ), are given as

$$\begin{aligned}\lambda &= \{\{\lambda_1\}, \{\lambda_2, \lambda_1\}, \dots, \{\lambda_k, \dots, \lambda_2, \lambda_1\}\}, \\ \mu &= \{\{\mu_1\}, \{\mu_1, \mu_2\}, \dots, \{\mu_1, \mu_2, \dots, \mu_k\}\}.\end{aligned}\quad (32)$$

For the tuples in (32), we introduce the associated generalized controllability and observability matrices, denoted with  $\mathcal{R} \in \mathbb{C}^{n \times k}$ , and respectively with  $\mathcal{O} \in \mathbb{C}^{k \times n}$ , as in Antoulas et al. (2016a), (Antoulas, 2005, chap. 4).

Given the above notations, we introduce the following matrices, *i.e.*, the generalized Loewner matrix  $\mathbb{L}$ , and the generalized shifted Loewner matrix  $\mathbb{M}$

$$\mathbb{L} = -\mathcal{O} \mathbf{E} \mathcal{R} \in \mathbb{C}^{k \times k}, \quad \mathbb{M} = -\mathcal{O} \mathbf{A} \mathcal{R} \in \mathbb{C}^{k \times k}. \quad (33)$$

In addition, we define matrices  $\mathbb{T} = \mathcal{O} \mathbf{N} \mathcal{R} \in \mathbb{C}^{k \times k}$ ,  $\mathbb{V} = \mathcal{O} \mathbf{B} \in \mathbb{C}^k$ , and  $\mathbb{W} = \mathbf{C} \mathcal{R} \in \mathbb{C}^{1 \times k}$ . Note that  $\mathbb{L}$  and  $\mathbb{M}$  as defined above are indeed Loewner matrices, that is, they can be expressed as divided differences of appropriate transfer function values of the underlying bilinear system; the following equalities hold:

$$\mathbb{L}(j, i) =$$

$$\frac{\mathbf{H}_{j+i-1}(\mu_1, \dots, \mu_j, \lambda_{i-1}, \dots, \lambda_1) - \mathbf{H}_{j+i-1}(\mu_1, \dots, \mu_{j-1}, \lambda_i, \dots, \lambda_1)}{\mu_j - \lambda_i}$$

$$\mathbb{M}(j, i) =$$

$$\frac{\mu_j \mathbf{H}_{j+i-1}(\mu_1, \dots, \mu_j, \lambda_{i-1}, \dots, \lambda_1) - \lambda_i \mathbf{H}_{j+i-1}(\mu_1, \dots, \mu_{j-1}, \lambda_i, \dots, \lambda_1)}{\mu_j - \lambda_i},$$

while  $\mathbb{V}(j, 1) = \mathbf{H}_j(\mu_1, \dots, \mu_{j-1}, \mu_j)$ ,  $\mathbb{W}(1, i) = \mathbf{H}_i(\lambda_i, \lambda_{i-1}, \dots, \lambda_1)$ , and  $\mathbb{T}(j, i) = \mathbf{H}_{j+i}(\mu_1, \dots, \mu_{j-1}, \mu_j, \lambda_i, \lambda_{i-1}, \dots, \lambda_1)$ . This result shows that all quantities of the bilinear Loewner surrogate model can be indeed computed using only data, and the realization is written concisely as

$$\hat{\mathbf{E}} = -\mathbb{L}, \quad \hat{\mathbf{A}} = -\mathbb{M}, \quad \hat{\mathbf{N}} = \mathbb{T}, \quad \hat{\mathbf{B}} = \mathbb{V}, \quad \hat{\mathbf{C}} = \mathbb{W}. \quad (34)$$

It was shown in Antoulas et al. (2016a), that the bilinear model of dimension  $k$  in (34) matches a total of  $2k + k^2$  transfer function values of the original bilinear system of dimension  $n$ . If necessary, the model given in (34) is further reduced similarly to the classical linear case, *e.g.*, as in (10). This is done by projecting with special matrices using the singular value decay of the Loewner pencil involved. This provides a useful indicator for choosing the truncation order (Antoulas et al., 2016a).

**Example 5** (Viscous (bi)linearized Burgers' equation model). We consider a discretized model of the viscous Burgers' equation (previously presented also in Antoulas et al. (2016a)). The original partial differential equation is given by

$$\frac{\partial v(x, t)}{\partial t} + v(x, t) \frac{\partial v(x, t)}{\partial x} = \frac{\partial}{\partial x} \left( v \frac{\partial v}{\partial x} \right), \quad (x, t) \in (0, 1) \times (0, T), \quad (35)$$

with initial and boundary conditions  $v(x, 0) = f(x)$ ,  $x \in [0, 1]$ ,  $v(0, t) = u(t)$ ,  $v(1, t) = 0$ ,  $t \geq 0$ . The viscosity coefficient  $\nu(x, t) = \nu$  is assumed to be constant and we consider zero initial conditions. Finally, we assume that the left boundary is subject to a control.

Start with a spatial discretization of Eq. (35), using an equidistant step size  $h = \frac{1}{n+1}$  where  $n$  denotes the number of interior points of the interval  $(0, 1)$ . By using first-order derivative approximations schemes, a nonlinear model is obtained (with quadratic-bilinear nonlinearities). Next, use the Carleman bilinearization technique to approximate this  $n^{\text{th}}$  order nonlinear system with a bilinear system of order  $\mathcal{N} = n^2 + n$ .

Denote with  $\mathcal{S}_B$  the  $4970^{\text{th}}$  order initial bilinear system obtained by means of the Carleman bilinearization. The first step is to collect samples from generalized bilinear transfer functions up to order two; the 400 interpolations points are chosen logarithmically spaced in the interval  $[10^{-3}, 10^3]$ . Next, we construct the bilinear Loewner matrices as presented in this section, and display the singular value decay in the left pane of Fig. 4. We construct a reduced-order model of order  $r = 32$ ; the poles are depicted in the right pane of Fig. 4.

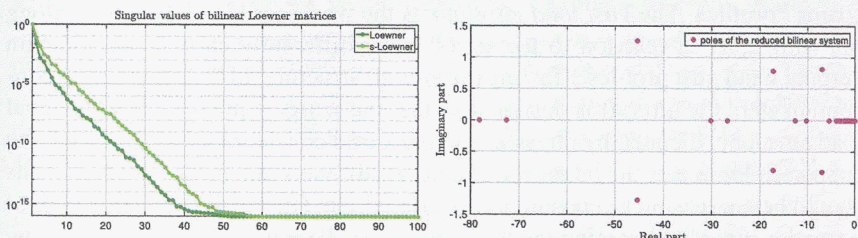


**FIGURE 4** The first 100 sv's of the Loewner matrices (left) and the poles of the ROM (right).

Finally, perform time-domain simulation for a control input given by  $u(t) = \frac{1}{5}(\cos(2\pi t) + \sin(20\pi t)e^{-t/5})$ , on time span  $[0, 10]$ s. The observed outputs for both the original and of the reduced-order bilinear systems are displayed in the left pane of Fig. 5, while the error is depicted in the right pane of Fig. 5.

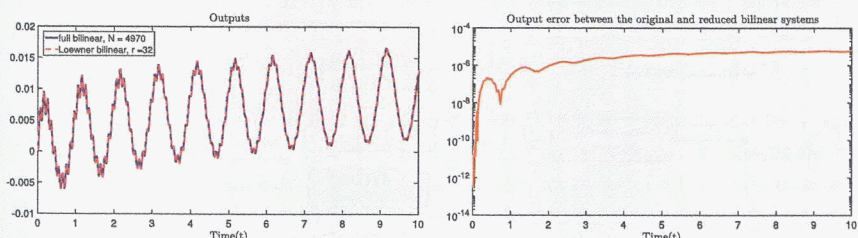


**FIGURE 5** The observed outputs (left) and the approximation error in the time domain (right).

### 3 Model reduction examples (large-scale systems)

In this section, we illustrate how Loewner-based rational approximation and reduction features have been successfully applied to real-life industrial problems. First, two benchmarks sequentially involving a generic business jet aircraft model and measurements data obtained by Dassault-Aviation, a French aircraft supplier, are considered (Meyer et al., 2017; Poussot-Vassal et al., 2021c). Second, a benchmark involving a simplified open channel model constructed by Electricité De France, the French electricity supplier is involved (Dalmas et al., 2016). A gust oriented model described by a non-rational transfer function is considered (Section 3.1), ground vibration experimental data (Section 3.2), and a linear partial differential equation (Section 3.3).

#### 3.1 Gust load oriented generic business jet aircraft model

The *gust load envelope* monitoring, is an important element to guarantee in aircraft structural integrity. One important certificate is to preserve and limit the worst case loads along the wings in response to vertical gust episodes. To this aim, we consider vertical gust disturbances  $w$ , modeled through the so-called “1-cosine” profiles. The *gust load envelope* is the worst case load responses along the wing span in reaction to the set of many differently chosen time-domain vertical wind gust profiles affecting the aircraft structure. In the preliminary conception step, the aircraft is designed so that the wings support a given nominal load envelope, dictated by physical and industrial considerations. The larger the supported loads are, the larger the structural stiffeners and mass reinforcements should be, increasing its consumption during flight. Gust load alleviation (**GLA**) control is aimed at lowering the loads envelope. To achieve this **GLA** function, as illustrated in Fig. 6, model-based control design approaches are usually preferred. Following Poussot-Vassal et al. (2021c), we illustrate through a generic business jet aircraft model constructed by Dassault-Aviation, how the Loewner framework is a pivotal tool used in the industry to simplify the complexity of these dynamical models, prior control design and analysis.

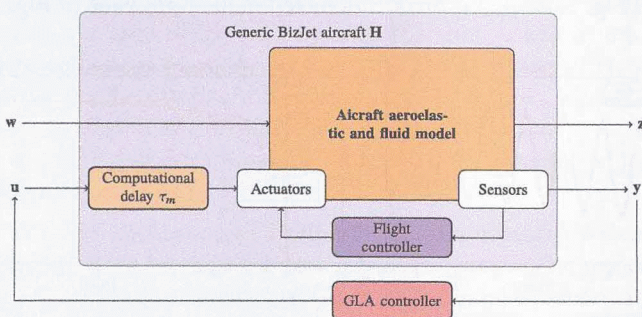


**FIGURE 6** Closed-loop architecture of the **GLA** problem.

At each flight and mass configuration, a linear dynamical model is constructed. Generic aircraft models have the following continuous-time realization  $\mathcal{S}$

$$\begin{aligned}\mathbf{E}\dot{\mathbf{x}}(t) &= \mathbf{A}_0\mathbf{x}(t) + \mathbf{A}_1\mathbf{x}(t - \tau_1) + \mathbf{A}_2\mathbf{x}(t - \tau_2) + \mathbf{B}_u\mathbf{u}(t) + \mathbf{B}_w\mathbf{w}(t), \\ \mathbf{y}(t) &= \mathbf{C}_0\mathbf{x}(t) + \mathbf{C}_1\mathbf{x}(t - \tau_m)\end{aligned}\quad (36)$$

where  $\mathbf{E}, \mathbf{A}_0, \mathbf{A}_1, \mathbf{A}_2 \in \mathbb{R}^{n \times n}$ ,  $\mathbf{B}_u \in \mathbb{R}^{n \times n_u}$ ,  $\mathbf{B}_w \in \mathbb{R}^{n \times n_w}$ ,  $\mathbf{C}_0, \mathbf{C}_1 \in \mathbb{R}^{p \times n}$  and  $\mathbf{x}(t) \in \mathbb{R}^n$ ,  $\mathbf{u}(t) \in \mathbb{R}^{n_u}$ ,  $\mathbf{w}(t) \in \mathbb{R}^{n_w}$  ( $m = n_u + n_w$ ) and  $\mathbf{y}(t) \in \mathbb{R}^p$  are the internal variables, control input, exogenous gust input and output signals, respectively. In the considered case,  $n_u = 3$ ,  $n_w = 1$  ( $m = 4$ ),  $p = 5$ , and  $n \approx 500$ . The presence of internal delays is caused by the physical restitution of the gust impact over the fuselage at three different locations function of the aircraft velocity. Moreover, due to the model construction method (see *e.g.* Quero et al. (2021) or Poussot-Vassal et al. (2021c)), the  $\mathbf{E}$  matrix may also be rank deficient. Here, due to the additional double derivative and delay structure added to accurately describe the gust disturbance effect along the fuselage,  $\text{rank } \mathbf{E} = n - 6$ . Following (36), the gust load model transfer associated function  $\mathbf{H}$ , from  $[\mathbf{u}^T, \mathbf{w}^T]^T$  to  $\mathbf{y}$  thus reads,  $\mathbf{H}(s) = (\mathbf{C}_0 + \mathbf{C}_1 e^{-\tau_m s})(s\mathbf{E} - \mathbf{A}_0 - \mathbf{A}_1 e^{\tau_1 s} - \mathbf{A}_2 e^{\tau_2 s})^{-1} \mathbf{B} \in \mathbb{C}^{p \times m}$ . We seek a simplified rational and polynomial model description to be used in place of  $\mathbf{H}(s)$  for fast simulation, control design and (modal) analysis. The first step in the process consists in gridding the interpolation (support points) along the imaginary axis and collecting the associated response (with  $\bar{n} = \underline{n} = n = 500$ ,  $2n = N$ , and  $\omega_i \neq \omega_j$ ):  $\{z_k\}_{k=1}^N = \{i\omega_i, -i\omega_i\}_{i=1}^{n/2} \cup \{i\omega_j, -i\omega_j\}_{j=1}^{n/2}$  and  $\{\Phi_k\}_{k=1}^N = \{\Phi_i, -\overline{\Phi_i}\}_{i=1}^{n/2} \cup \{\Phi_j, -\overline{\Phi_j}\}_{j=1}^n$ , where  $\omega_i, \omega_j \in \mathbb{R}_+$  are the frequencies at which one evaluates each transfer  $\mathbf{H}$ . In our application, the  $\omega_i, \omega_j$ 's are logarithmically spaced.

**Remark 6** (About a Padé approximation). One option is to replace the delays with a Padé approximation. This preserves the gain but modifies the phase. While this is classically used in many applications, it is, to the authors experience, not the most accurate way to deal with internal and external delays. Indeed, Padé often results in significant error in the phase, which can be inappropriate for flexible structures. In addition, Padé will drastically increase the model internal dimension which in turn is not appropriate for model reduction. The accuracy / complexity ratio is not in favor of Padé (see also Fig. 7).

Fig. 7 illustrates the transfer function from the gust disturbance to a wing bending moment output, used to monitor the gust envelope. It compares the responses of the original irrational model  $\mathbf{H}$  with its rational approximate model  $\mathbf{H}_n$  constructed with Loewner matrices and its rational approximation obtained with Padé  $\mathbf{H}_{\text{Padé}}$ .

Fig. 7 emphasizes the good performance of the rational model obtained after reducing the complexity of the model. The phase is much well captured

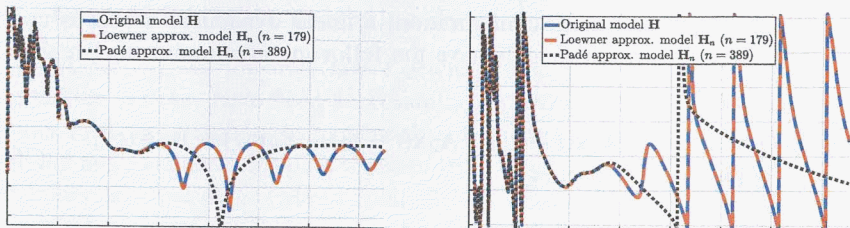


**FIGURE 7** Left: frequency response gain. Right: frequency phase response. Comparison of the original model with the rational approximation obtained by Loewner and Padé.

by the Loewner approach than with Padé, while using less internal variables. In Poussot-Vassal et al. (2021c), this rational model is then used for **GLA** controller synthesis, leading to a load envelope reduction which is achievable thanks to the Loewner framework.

### 3.2 Ground vibration tests on business jet aircraft

We continue on the business aircraft benchmark provided by Dassault-Aviation, moving to the vibration problem, related to fatigue and comfort issues. Anti-vibration controllers are designed using model, targeting undesirable amplifications of the aerodynamical effects on the fuselage around some specified frequencies (Poussot-Vassal et al., 2013). After control design, Ground Vibration Tests (**GVT**) are performed to both validate the control performances and the original model. The benchmark considered here illustrates the generic business jet **GVT**, performed on a Falcon 7X at Istres, France, in 2015 (Meyer et al., 2017).

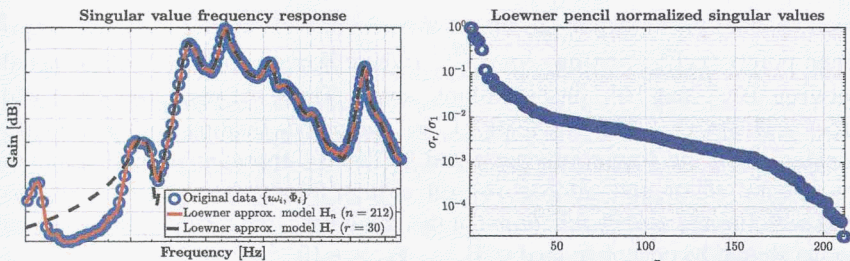
Dassault-Aviation engineers implemented the control law on the real business jet aircraft. Then, using shakers applied at some aircraft locations, the structure was excited, thus simulating aerodynamic disturbances. Hundreds of sensors were positioned on the aircraft and used for analysis.<sup>7</sup>

Fig. 8 (left) shows the singular frequency response of the (open-loop) data collected between a single-input and 100-outputs, compared with the frequency response of a rational models (with different complexity). The singular values drop is also illustrated on Fig. 8 (right).

In this industrial case, the Loewner framework is shown to be able to accurately recover the transfer function from raw data. It allows engineers to re-adjust the theoretical models with experiments, to detect some new phenomena and re-tune the control laws. This step contributes to the quest for a so-called *digital twin*.<sup>8</sup>

<sup>7</sup> [https://drive.google.com/file/d/1H2Gq1Ykiny\\_PZND2ekB6swSetoGcmFTK/view](https://drive.google.com/file/d/1H2Gq1Ykiny_PZND2ekB6swSetoGcmFTK/view) video illustrates the kinematic effect of the control law acting on the tail surface to reduce the vibrations.

<sup>8</sup> Additional information may be found in Meyer et al. (2017) or in §2.4.7 of Poussot-Vassal (2019).



**FIGURE 8** Left: singular value frequency response of the data (dotted blue), minimal McMillan degree model (solid orange) and 30-th order model (dashed black). Right: Loewner singular values.

### 3.3 Hydroelectricity open-channel benchmark

Let consider a model representing the level  $h$  of an open-channel as a function of the inflow  $q_i$  and outflow  $q_o$  inputs. Such a model is used by hydro-electricity engineers from Electricité De France to monitor the level of a river in order to control the available energy. In France, in May 2021, the hydraulic energy represented about 10% of the total produced energy. These models in such benchmarks belong to the class of linear partial differential equations (**PDE**), coming from two nonlinear hyperbolic Saint-Venant equations, given as:

$$\frac{\partial S}{\partial t} + \frac{\partial Q}{\partial x} = 0 \text{ and } \frac{\partial Q}{\partial t} + \frac{\partial (Q^2/S)}{\partial x} + gS \frac{\partial H}{\partial x} = gS(I - J), \quad (37)$$

where  $x \in [0, L]$  is the spatial variable,  $t$  the time variable,  $H(x, t)$  the water depth,  $S(x, t)$  the wetted area,  $Q(x, t)$  the discharge,  $g$  the gravity acceleration and  $J$  the Manning-Strickler friction.<sup>9</sup> Under mild assumptions a linearization around an equilibrium point  $(Q_0, H_0)$ , detailed in Dalmas et al. (2016), expresses the variation relations  $(q, h)$ , between inflow ( $q_e$ , being  $q$  at  $x = 0$ ), outflow ( $q_s$ , being  $q$  at  $x = L$ ) and the water depth ( $h$ , at a given measurement point  $x$ ) as follows,  $h(x, s) = \mathbf{G}_e(x, s)q_e(s) - \mathbf{G}_s(x, s)q_s(s)$ , where

$$\begin{aligned} \mathbf{G}_i(x, s) &= \frac{\lambda_1(s)e^{\lambda_2(s)L+\lambda_1(s)x} - \lambda_2(s)e^{\lambda_1(s)L+\lambda_2(s)x}}{B_0s(e^{\lambda_1(s)L} - e^{\lambda_2(s)L})} \text{ and} \\ \mathbf{G}_o(x, s) &= \frac{\lambda_1(s)e^{\lambda_1(s)x} - \lambda_2(s)e^{\lambda_2(s)x}}{B_0s(e^{\lambda_1(s)L} - e^{\lambda_2(s)L})}. \end{aligned} \quad (38)$$

For a frozen measurement point  $x = x_m$ , one has  $h_{x_m}(s) = \mathbf{H}(s)\mathbf{u}(s) = \mathbf{G}_i(x_m, s)q_i(s) + \mathbf{G}_o(x_m, s)q_o(s)$ , where  $\mathbf{u}(s)$  contains the  $q_i(s)$  and  $q_o(s)$  and where  $\mathbf{H}$  is now a one output two inputs complex-valued transfer function. Fig. 9 illustrates the approximation features and accurate reconstruction of the

<sup>9</sup> Numerical values of this model are provided at [https://morwiki.mpi-magdeburg.mpg.de/morwiki/index.php/Hydro-Electric\\_Open\\_Channel](https://morwiki.mpi-magdeburg.mpg.de/morwiki/index.php/Hydro-Electric_Open_Channel).

open-channel phenomenon. To obtain this result, we consider complex conjugated points  $\{z_k\}_{k=1}^N = \{\imath\omega_k, -\imath\omega_k\}_{k=1}^{N/2}$  (where  $\bar{n} = \underline{n} = 300 = N/2$ ) sampled between  $10^{-4}$  and  $10^{1.5}$  in logarithmic space. Then, the responses  $\mathbf{H}(s)$  and  $\tilde{\mathbf{H}}(s) = \mathbf{H}(s)s/(s + 10^{-2})(s + 10^{-3})$ , are computed. Dealing with  $\tilde{\mathbf{H}}$  remains standard with the framework presented so far. By approximating  $\tilde{\mathbf{H}}$  removes the integral action and enforces roll-off in high frequency, and thus allows to deal with limited energy functions. In this latter case, the resulting interpolated model should be post processed as  $\tilde{\mathbf{H}}_n \leftarrow \mathbf{H}_n(s + 10^{-2})(s + 10^{-3})/s$  to recover the original one.

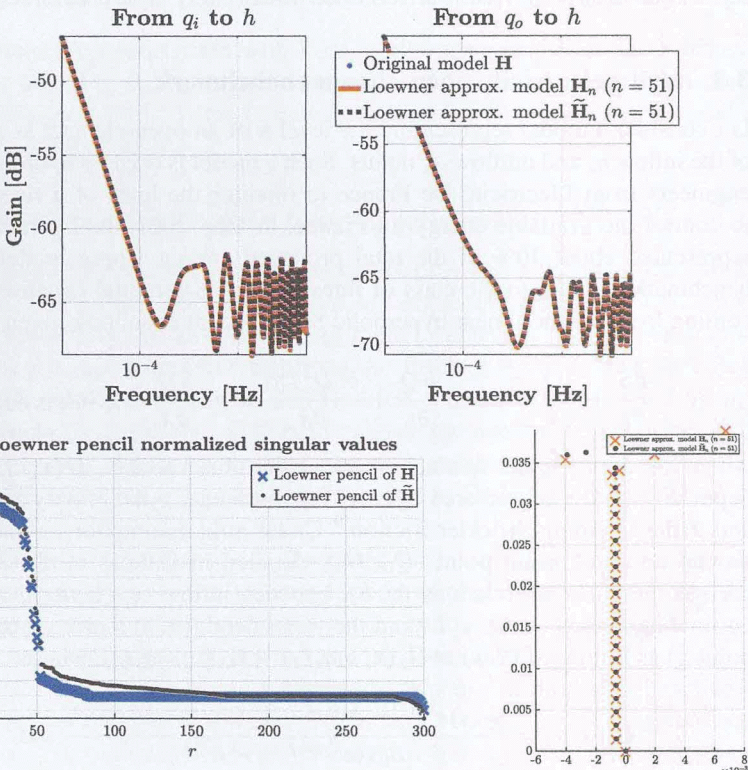


**FIGURE 9** Top: frequency response comparison between the original irrational model and two approximated Loewner models. Bottom left: Singular values drop of the Loewner pencil for the two models. Bottom right: eigenvalues of the resulting minimal order rational approximation.

Both approaches lead to a perfect matching of the irrational transfer. Interestingly, working with  $\tilde{\mathbf{H}}$  instead of  $\mathbf{H}$  leads to a model with all singularities on the left hand side plus the 0 one. Working with the shifted function  $\tilde{\mathbf{H}}$  illustrates how one can perform gray box identification by simply shifting the original data. Here, the integral action (physically known from open-channel models) is removed and added afterward.

## 4 Control in the Loewner framework

Let us now deviate from the original purpose of the Loewner framework, initially introduced to provide solutions to the identification, approximation and reduction problems through the lens of rational and polynomial function construction. Here instead, Loewner is used for feedback controller design. More specifically it is used as in some traditional loop shaping methods, to fit a reference controller. In the proposed setup, the reference controller is not computed by means of a model but in terms of input-output data. Two applications are illustrated. The first one involves experimental data and considers the design of a reference tracking controller applied on a pulsed fluidic actuator (**PFA**), see Section 4.2, (Poussot-Vassal et al., 2021a). The second considers a numerical benchmark representing the boundary control a wave equation, described by an infinite dimensional equation.

### 4.1 Data-driven control, virtual reference model and L-DDC rationale

In this section, the Loewner framework is used for synthesizing a controller directly from measured data, being then a data-driven control (**DDC**) framework.<sup>10</sup> **DDC** consists in recasting the control design problem as an identification one. The technique under consideration belongs to the so-called *reference model approaches* and more specifically relies on the definition of a so-called *ideal controller*, derived from a reference model. This framework is deployed in the frequency-domain, with the use of the Loewner framework as the identification tool in Kergus et al. (2017); Vuillemin et al. (2020), allowing to skip the controller complexity selection thanks to its rank properties (see Section 2). The Loewner data-driven control (**L-DDC**) is thus a combination of determining the ideal controller from frequency-domain data via a reference model and the use of the Loewner framework (Mayo and Antoulas, 2007) to construct a reduced order controller. Such an interpolatory-based data-driven control design solves problems faced by practitioners: (*i*) the controller design is directly obtained using open-loop raw data collected on the experimental setup, (*ii*) without any prior controller structure or order specification.

The **L-DDC** procedure boils down to two steps: first deriving the *ideal controller* definition and second the *controller identification* via interpolation in the Loewner framework. We recall the mains steps in the **SISO** case. Following Fig. 10, the objective is to find a controller with transfer function  $\mathbf{K} : \mathbb{C} \setminus \Lambda_{\mathbf{K}} \rightarrow \mathbb{C}$  that minimizes the difference between the resulting closed-loop and a given user-defined reference model  $\mathbf{M} : \mathbb{C} \setminus \Lambda_{\mathbf{M}} \rightarrow \mathbb{C}$ . This is made possible through the definition of the ideal controller  $\mathbf{K}^*$ , being the **LTI** controller that would have given the desired reference model behavior if inserted

---

<sup>10</sup> The reader may notice that **DDC** methods have a long history dating to the proportional, integral, derivative (**PID**) tuning method by Ziegler-Nichols in early 40's or the self tuning regulator by Åström in the 90's (see e.g. Ziegler and Nichols, 1942 for more details and references).

in the closed-loop. The latter is defined as  $\mathbf{K}^* = \mathbf{H}^{-1}\mathbf{M}(I - \mathbf{M})^{-1}$ . In the data-driven case, this definition may be recast as a discrete set of equations (where  $\{z_k\}_{k=1}^N \in \mathbb{C}$ ,  $k = 1, \dots, N$ )

$$\mathbf{K}^*(z_k) = \mathbf{H}(z_k)^{-1}\mathbf{M}(z_k)(I - \mathbf{M}(z_k))^{-1}, \quad (39)$$

where  $\mathbf{H}(z_k)$  is the evaluation of the considered model, if available. In an experimental context, one usually considers sampling  $\mathbf{H}$  at  $z_k = i\omega_k$  ( $\omega_k \in \mathbb{R}_+$ ). Finding a controller  $\mathbf{K}$  that fits  $\mathbf{K}^*(z_k)$  can be considered to be an identification problem. In the Loewner framework, the control design boils down to finding a transfer function  $\mathbf{K}$  satisfying condition (39).

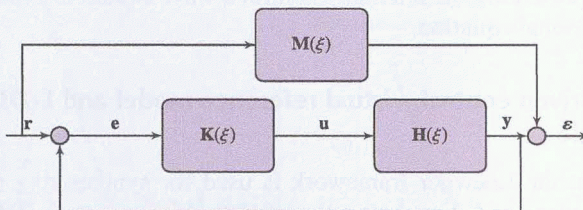


FIGURE 10 Data-driven control problem formulation.

## 4.2 Pulsed fluidic actuator control

The design of active closed-loop flow controllers constitutes an important field of research in fluid mechanics (Sipp and Schmid, 2016). In most contributions, both the sensor(s) and the actuator(s) are supposed to be lumped and ideal. To move towards experimental applications and real-life validations, it is essential to consider realistic set-ups and is the core contribution of Poussot-Vassal et al. (2021a), where the L-DDC is applied on a PFA. PFA are on/off actuators that blow air to modify the pressure in a flow setup. The control setup considered is schematized on Fig. 11.

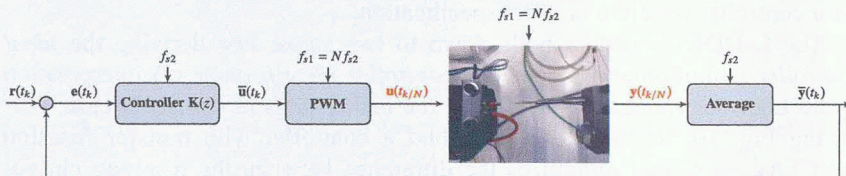
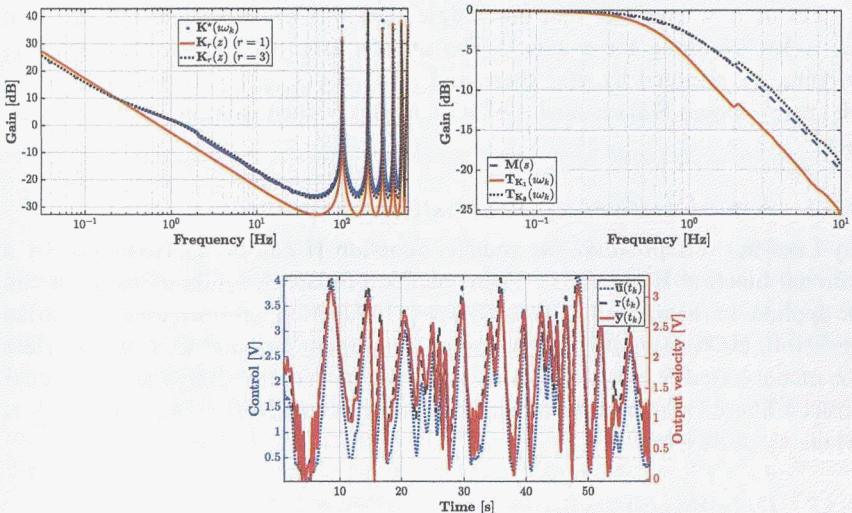


FIGURE 11 PFA control setup (details are in Poussot-Vassal et al., 2021a).

After exciting the PFA using a pseudo random binary sequence  $\mathbf{u}(t_{k/N})$ , output data  $\mathbf{y}(t_{k/N})$  are collected. The corresponding frequency responses  $\bar{\mathbf{u}}$  and  $\bar{\mathbf{y}}$  are computed and transfer function values  $\mathbf{H}(i\omega_k)$  are thus obtained. Applying (39) with  $z_k = i\omega_k$  and the Loewner approach, it leads to a singular value

decay indicating that a first or third order model is sufficient to recover the main dynamics (see Fig. 12). One important result is the ability of the **L-DDC** to construct, directly from raw open-loop data, a control law performing well on an experimental setup. Relevant in this context is that the **L-DDC** structure and complexity is almost automatically chosen by the Loewner framework, and no pole pre-assignment is required.



**FIGURE 12** Top left: gain of the frequency responses of the ideal controller  $\mathbf{K}^*$  (blue dots) and of the estimated controller  $\tilde{\mathbf{K}}_r(s)$  of order  $r = 1$  (solid orange) and  $r = 3$  (dotted black). Top right: closed-loop response estimation using controller  $\mathbf{K}_1$  and  $\mathbf{K}_3$  of the averaged output  $\bar{y}(t_k)$  (solid orange and dotted black). Bottom: time-domain closed-loop response to a reference trajectory  $\mathbf{r}(t_k)$  (dashed black), averaged control signal  $\bar{u}(t_k)$  (dotted blue) and averaged output (solid orange).

### 4.3 Transport phenomena benchmark

Let us consider the case of a one dimensional transport equation controlled at its left boundary through a second order actuator. This model is used in Poussot-Vassal et al. (2021b) and detailed in §2, Example 7 of Poussot-Vassal (2019). This phenomenon is represented by a linear **PDE** with constant coefficients interconnected with a second order linear **ODE** actuator, as described in (40).

$$\frac{\partial \tilde{y}(x, t)}{\partial x} + 2x \frac{\partial \tilde{y}(x, t)}{\partial t} = 0, \quad \tilde{y}(x, 0) = 0 \text{ and } \tilde{y}(0, t) = \frac{1}{\sqrt{t}} \tilde{u}_f(0, t) \quad (40)$$

where  $\omega_0^2/(s^2 + m\omega_0 s + \omega_0^2)u(0, s) = u_f(0, s)$  and  $x \in [0, L]$  ( $L = 3$ ) is the spatial variable. Then,  $\omega_0 = 3$  and  $m = 0.5$  are the input actuator parameters. The scalar model input is the vertical force applied at the left boundary, *i.e.* at  $x = 0$ . We denote the input  $\tilde{u}(0, t)$  in the time-domain or  $\mathbf{u}(0, s)$  in the complex

one. Similarly, the output at location  $x$  is given as  $\tilde{\mathbf{y}}(x, t)$  for the time-domain and  $\mathbf{y}(x, s)$  in the complex one. By applying the Laplace transform, one obtains the transfer function from the input  $\mathbf{u}(0, s)$  to the output  $\mathbf{y}(x, s)$ :

$$\mathbf{y}(x, s) = \frac{\sqrt{\pi}}{\sqrt{s}} e^{-x^2 s} \frac{\omega_0^2}{s^2 + m\omega_0 s + \omega_0^2} \mathbf{u}(0, s) = \mathbf{G}(x, s) \mathbf{u}(0, s). \quad (41)$$

Let us now consider that one single sensor is available and is located at  $x_m = 1.9592$  along the  $x$ -axis.<sup>11</sup> The transfer from  $\mathbf{u}(0, s)$ , denoted by  $\mathbf{u}(s)$  to  $\mathbf{y}(x_m, s)$ , denoted by  $\mathbf{y}(s)$  then reads  $\mathbf{y}(s) = \mathbf{y}(x_m, s) = \mathbf{G}(s, x_m) \mathbf{u}(0, s) = \mathbf{H}(s) \mathbf{u}(s)$ , where  $\mathbf{H}(s)$  is now a **SISO** complex-valued irrational transfer function.

#### 4.3.1 A model-driven approximation and control

By Loewner interpolation, the transfer function  $\mathbf{H}$  can be approximated by a rational function  $\mathbf{H}_r$  ( $r = 33$ ). Then, standard feedback synthesis methods can be applied. In this example, the **HINSTRUCT** function has been used (Apkarian and Noll, 2006). Details may be found in Poussot-Vassal et al. (2021b). Here the model-based  $\mathcal{H}_\infty$ -norm minimization oriented control design allows to construct a filtered proportional integral (**PI**) of the form  $\mathbf{K}(s) = (k_p + k_i \frac{1}{s}) \frac{1}{s/a+1}$ , where  $k_p, k_i, a \in \mathbb{R}$ .

#### 4.3.2 Data-driven control

Let us now apply the **L-DDC** rationale, instead of a model-based control design. The reference model choice is a key factor for the **L-DDC** success, as for any other model reference control procedure. Indeed, the latter should not only represent a desirable closed-loop behavior, but also achievable dynamics of the considered system (*i.e.* the ideal controller should not internally destabilize the plant). A reference model is said to be achievable by the plant if the corresponding ideal controller internally stabilizes the plant. Here let us skip this point and focus on the equivalence of model vs. data-based design. Let the reference model  $\mathbf{M}$  be the closed-loop rational function obtained by the previous approach interconnecting  $\mathbf{H}_r$  with the obtained filtered **PI** control law obtained in the above section.

By computing the ideal controller through (39), we again compute the Loewner pencil, leading to a minimal realization with  $n = 42$ . Obviously, such a control order is prohibitive for classical control applications. The singular values decay indicates that an order  $r = 2$  is enough to catch the main dynamics of the underlying controller. One obtains transfer function  $\mathbf{K}_2(s) = (1082.7(s + 0.1313))/(s(s + 5656))$ , being close to the values obtained by the

---

<sup>11</sup> In the rest of the chapter,  $x$  will be discretized with 50 points from 0 to  $L = 3$ , and  $x_m$  has been chosen to be located at  $x(\lfloor 50 \times 2/3 \rfloor)$ .

model-based approach.<sup>12</sup> The controller and resulting close-loop frequency response gains are shown in Fig. 13.

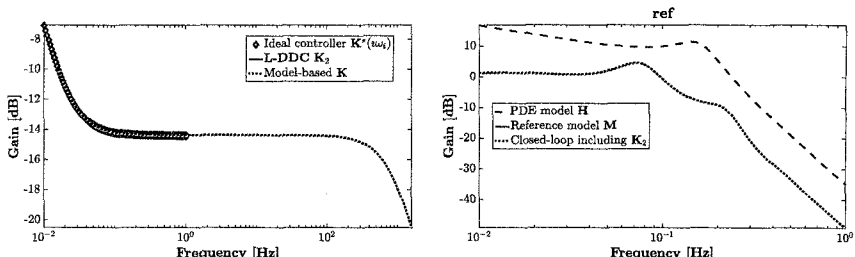


**FIGURE 13** Left: frequency response of the controller (ideal, model-based and data-driven). Right: open-loop vs. closed-loop frequency responses.

Interestingly, with reference to Fig. 13,  $\mathbf{K}_r$  perfectly recovers the model-based requested performances of  $\mathbf{M}$  with a controller of rational order two (indeed, we expected to observe this result since we knew from the model-based approach presented in Section 4.3.1 that a rational control of this order leading to this performance is achievable).

This example demonstrates how the Loewner framework can be effectively used, either for model-based, or for data-driven control. Interestingly, by choosing the closed-loop performances  $\mathbf{M}$  obtained with the model-based approach, the controller  $\mathbf{K}_r$  exactly recovers the original properties, while skipping the model construction step and the order selection. This property reduces the model construction step and allows a quick design of the controller. However, this main advantage is balanced by the fact that in the model-based approach, the stability assessment is usually carried out using the approximate model, here  $\mathbf{H}_r$ . The latter being very accurate, the eigenvalues computation is traditionally enough for concluding stability. On the contrary, in the second data-driven approach, stability cannot be analyzed as easily. Still, Poussot-Vassal et al. (2021b) suggests an approach based on the combination of Loewner with optimal  $\mathcal{H}_\infty$  projections.

Finally, we mention that all numerical experiments reported in this manuscript were performed on a laptop computer with the following specifications: 16 GB RAM and an Intel(R) Core(TM) i7-10510U CPU running at 1.80 GHz 2.30 GHz, while the software platform used was MATLAB® R2019a.

## 5 Summary and conclusions

In this work, we have provided an inventory of selected extensions and applications of the Loewner framework. The main philosophy of this approach is as follows: use the available data to construct a model or a controller; if needed, apply compression techniques to reduce the complexity of the model

<sup>12</sup> The model based approach yield to  $1084.9(s + 0.1313)/s(s + 5667)$ .

or of the controller. The Loewner framework was shown to be applicable for reducing large-scale dynamical systems from computational fluid dynamics (such as the linearized Navier-Stokes model with more than half a million degrees of freedom), to data-driven modeling in aeronautics applications, and to various benchmarks described by complicated dynamics (characterized by irrational transfer functions, having multiple delays, with many input or output ports, with nonlinear terms etc.). The key observation here is that one can accomplish all of these successful endeavors by having access only to compressed data (transfer function measurements, Markov parameters, etc.). Moreover, the Loewner data-driven control approach was shown to faithfully recover the performance attained by other classical model-based control approaches. Thus, one advantage is the data-driven characteristic, and another is the robustness of the approach. The Loewner framework is hence a valid alternative to intrusive methodologies, and can be successfully used when data are available.

## References

- Antoulas, A.C., 2005. Approximation of Large-Scale Dynamical Systems. SIAM, Philadelphia.
- Antoulas, A.C., Anderson, B.D.O., 1986. On the scalar rational interpolation problem. *IMA Journal of Mathematical Control and Information* 3 (2–3), 61–88.
- Antoulas, A.C., Beattie, C.A., Gugercin, S., 2020a. Interpolatory Methods for Model Reduction. Society for Industrial and Applied Mathematics, Philadelphia.
- Antoulas, A.C., Gosea, I.V., Heinkenschloss, M., 2019. On the Loewner framework for model reduction of Burgers' equation. In: King, R. (Ed.), Active Flow and Combustion Control, Notes on Numerical Fluid Mechanics and Multidisciplinary Design. Springer, Cham, Switzerland, pp. 255–270.
- Antoulas, A.C., Gosea, I.V., Heinkenschloss, M., 2020b. Reduction of systems with polynomial nonlinearities in the Loewner framework. In: Book of Abstracts of XXI Householder Symposium on Numerical Linear Algebra. Selva di Fasano, Italy, June 14–19.
- Antoulas, A.C., Gosea, I.V., Ionita, A.C., 2016a. Model reduction of bilinear systems in the Loewner framework. *SIAM Journal on Scientific Computing* 38 (5), B889–B916.
- Antoulas, A.C., Ionita, A.C., Lefteriu, S., 2012. On two-variable rational interpolation. In: Special Issue dedicated to Danny Sorensen's 65th birthday. *Linear Algebra and Its Applications* 436 (8), 2889–2915.
- Antoulas, A.C., Lefteriu, S., Ionita, A.C., 2017. A tutorial introduction to the Loewner framework for model reduction. In: Model Reduction and Approximation. SIAM, pp. 335–376. Chapter 8.
- Antoulas, A.C., Zhu, B., Zhang, Q., York, B., O'Malley, B.W., Dacso, C., 2018. A novel mathematical method for disclosing oscillations in gene transcription: a comparative study. *PLoS ONE* 13 (9), 1–20.
- Apkarian, P., Noll, D., 2006. Nonsmooth  $\mathcal{H}_\infty$  synthesis. *IEEE Transactions on Automatic Control* 51 (1), 71–86.
- Barbagallo, A., Sipp, D., Schmid, P.J., 2008. Closed-loop control of an open cavity flow using reduced-order models. *Journal of Fluid Mechanics* 641, 1–50.
- Benner, P., Breiten, T., 2012. Interpolation-based  $\mathcal{H}_2$ -model reduction of bilinear control systems. *SIAM Journal on Matrix Analysis and Applications* 33, 859–885.
- Benner, P., Gugercin, S., Willcox, K., 2015. A survey of projection-based model reduction methods for parametric dynamical systems. *SIAM Review* 57 (4), 483–531.
- Benner, P., Ohlberger, M., Cohen, A., Willcox, K., 2017. Model Reduction and Approximation. Society for Industrial and Applied Mathematics, Philadelphia, PA.

- Berrut, J.-P., Trefethen, L.N., 2006. Barycentric Lagrange interpolation. *SIAM Review* 46 (3), 501–517.
- Breiten, T., Damm, T., 2010. Krylov subspace methods for model order reduction of bilinear control systems. *Systems & Control Letters* 59, 443–450.
- Carleman, T., 1932. Application de la théories des équations intégrales linéaires aux systèmes d'équations différentielles non linéaires. *Acta Mathematica* 59, 63–87.
- Dalmas, V., Robert, G., Poussot-Vassal, C., Pontes Duff, I., Seren, C., 2016. From infinite dimensional modelling to parametric reduced order approximation: application to open-channel flow for hydroelectricity. In: Proceedings of the 15th European Control Conference. Aalborg, Denmark, pp. 1982–1987.
- Flagg, G., Gugercin, S., 2015. Multipoint Volterra series interpolation and  $\mathcal{H}_2$  optimal model reduction of bilinear systems. *SIAM Journal on Matrix Analysis and Applications* 36 (2), 549–579.
- Gallivan, K.A., Vanderope, A., Van Dooren, P., 2004. Model reduction of MIMO systems via tangential interpolation. *SIAM Journal on Matrix Analysis and Applications* 26 (2), 328–349.
- Gosea, I.V., 2017. Model order reduction of linear and nonlinear systems in the Loewner framework. PhD thesis. Jacobs University Bremen.
- Gosea, I.V., Antoulas, A.C., 2015. Model reduction of linear and nonlinear systems in the Loewner framework: a summary. In: 14th European Control Conference (ECC). Linz, Austria, July 15–17, pp. 345–349.
- Gosea, I.V., Antoulas, A.C., 2016. Stability preserving post-processing methods applied in the Loewner framework. In: IEEE 20th Workshop on Signal and Power Integrity (SPI). Turin, Italy, May 8–11, pp. 1–4.
- Gosea, I.V., Antoulas, A.C., 2018. Data-driven model order reduction of quadratic-bilinear systems. *Numerical Linear Algebra with Applications* 25 (6), e2200.
- Gosea, I.V., Karachalios, D.S., Antoulas, A.C., 2021a. Learning reduced-order models of quadratic control systems from input-output data. In: Proceedings of the IEEE European Control Conference ECC, Virtual, pp. 1426–1431.
- Gosea, I.V., Poussot-Vassal, C., Antoulas, A.C., 2021b. On Loewner data-driven control for infinite-dimensional systems. In: Proceedings of the IEEE European Control Conference, Virtual, pp. 93–99.
- Gosea, I.V., Zhang, Q., Antoulas, A.C., 2020. Preserving the DAE structure in the Lowner model reduction and identification framework. *Advances in Computational Mathematics* 46 (3).
- Gugercin, S., Antoulas, A.C., Beattie, C.A., 2008.  $\mathcal{H}_2$  model reduction for large scale linear dynamical systems. *SIAM Journal on Matrix Analysis and Applications* 30 (2), 609–638.
- Ionita, A.C., Antoulas, A.C., 2012. Matrix Pencils in Time and Frequency Domain System Identification. Developments in Control Theory Towards Glocal Control. The Institution of Engineering and Technology. Chapter 9.
- Ionita, A.C., Antoulas, A.C., 2014. Data-driven parametrized model reduction in the Loewner framework. *SIAM Journal on Scientific Computing* 36 (3), A984–A1007.
- Karachalios, D.S., Gosea, I.V., Antoulas, A.C., 2020a. The Loewner framework for system identification and reduction. In: Benner, P., Grivet-Talocia, S., Quarteroni, A., Rozza, G., Schilders, W.H.A., Silveira, L.M. (Eds.), Methods and Algorithms. In: Handbook on Model Reduction, vol. 1. De Gruyter, pp. 181–228.
- Kergus, P., Poussot-Vassal, C., Demourant, F., Formentin, S., 2017. Frequency-domain data-driven control design in the Loewner framework. In: Proceedings of the 20th IFAC World Congress. Toulouse, France, pp. 2095–2100.
- Lefteriu, S., Antoulas, A.C., Ionita, A.C., 2011. Parametric model reduction in the Loewner framework. In: 18th IFAC World Congress. IFAC Proceedings Volumes 44 (1), 12751–12756.
- Ljung, L., 1987. System Identification: Theory for the User. Prentice Hall, Upper Saddle River, New Jersey. 2nd edition in 1999.
- Mayo, A.J., Antoulas, A.C., 2007. A framework for the solution of the generalized realization problem. *Linear Algebra and Its Applications* 425 (2–3), 634–662.

- Meyer, C., Broux, G., Prodigue, J., Cantinaud, O., Poussot-Vassal, C., 2017. Demonstration of innovative vibration control on a Falcon Business Jet. In: Proceedings of the International Forum on Aeroelasticity and Structural Dynamics. Como, Italy.
- Nakatsukasa, Y., Sete, O., Trefethen, L.N., 2018. The AAA algorithm for rational approximation. *SIAM Journal on Scientific Computing* 40 (3), A1494–A1522.
- Niconet, e.V., 2002. Benchmark examples for model reduction of linear time invariant dynamical systems.
- Peherstorfer, B., Gugercin, S., Willcox, K., 2017. Data-driven reduced model construction with time-domain Loewner models. *SIAM Journal on Scientific Computing* 39 (5), A2152–A2178.
- Poussot-Vassal, C., 2019. Large-scale dynamical model approximation and its applications. HDR, habilitation thesis. Onera, INP Toulouse, Toulouse, France.
- Poussot-Vassal, C., Kergus, P., Kerhervé, F., Sipp, D., Cordier, L., 2021a. Interpolatory-based data-driven pulsed fluidic actuator control design and experimental validation. In: *IEEE Transactions on Control Systems Technology*.
- Poussot-Vassal, C., Kergus, P., Vuillemin, P., 2021b. *Interpolation-Based Irrational Model Control Design and Stability Analysis*. Springer. In press. Preprint available arXiv:2012.01040.
- Poussot-Vassal, C., Leclercq, C., Sipp, D., 2018. Structured linear fractional parametric controller  $\mathcal{H}_\infty$  design and its applications. In: Proceedings of the European Control Conference. Limassol, Cyprus.
- Poussot-Vassal, C., Loquen, T., Vuillemin, P., Cantinaud, O., Lacoste, J.-P., 2013. Business jet large-scale model approximation and vibration control. In: Proceedings of the 11th IFAC ALCOSP. Caen, France, pp. 199–204.
- Poussot-Vassal, C., Sipp, D., 2015. Parametric reduced order dynamical model construction of a fluid flow control problem. In: Proceedings of the 1st IFAC Workshop on Linear Parameter Varying Systems. Grenoble, France, pp. 133–138.
- Poussot-Vassal, C., Vuillemin, P., Cantinaud, O., Sèze, F., 2021c. Interpolatory methods for generic BizJet gust load alleviation function. *SIAM Journal on Applied Dynamical Systems* 20 (4), 2391–2411.
- Quero, D., Vuillemin, P., Poussot-Vassal, C., 2021. A generalized eigenvalue solution to the flutter stability problem with true damping: the p-L method. *Journal of Fluids and Structures* 103, 103266.
- Rugh, W.J., 1981. *Nonlinear System Theory - the Volterra/Wiener Approach*. The Johns Hopkins University Press.
- Sipp, D., Schmid, P.J., 2016. Linear closed-loop control of fluid instabilities and noise-induced perturbations: a review of approaches and tools. *Applied Mechanical Revue* 68.
- Vuillemin, P., Kergus, P., Poussot-Vassal, C., 2020. Hybrid Loewner data driven control. In: Proceedings of the IFAC World Congress. Berlin, Germany.
- Ziegler, J.G., Nichols, N.B., 1942. Optimum settings for automatic controllers. *Transactions of the American Society of Mechanical Engineers* 64, 759–768.